



**HAL**  
open science

## Missing lawsonite and aragonite found: P–T and fluid composition in meta-marls from the Combin Zone (Western Alps)

Paola Manzotti, Michel Ballèvre, Pavel Pitra, Federica Schiavi

### ► To cite this version:

Paola Manzotti, Michel Ballèvre, Pavel Pitra, Federica Schiavi. Missing lawsonite and aragonite found: P–T and fluid composition in meta-marls from the Combin Zone (Western Alps). *Contributions to Mineralogy and Petrology*, 2021, 176 (8), pp.60. 10.1007/s00410-021-01818-0 . insu-03320510

**HAL Id: insu-03320510**

**<https://insu.hal.science/insu-03320510>**

Submitted on 24 Aug 2021

**HAL** is a multi-disciplinary open access archive for the deposit and dissemination of scientific research documents, whether they are published or not. The documents may come from teaching and research institutions in France or abroad, or from public or private research centers.

L'archive ouverte pluridisciplinaire **HAL**, est destinée au dépôt et à la diffusion de documents scientifiques de niveau recherche, publiés ou non, émanant des établissements d'enseignement et de recherche français ou étrangers, des laboratoires publics ou privés.



# Missing lawsonite and aragonite found: $P$ – $T$ and fluid composition in meta-marls from the Combin Zone (Western Alps)

Paola Manzotti<sup>1</sup> · Michel Ballèvre<sup>2</sup> · Pavel Pitra<sup>2,3</sup> · Federica Schiavi<sup>4</sup>

Received: 22 March 2021 / Accepted: 12 July 2021 / Published online: 26 July 2021  
© The Author(s) 2021

## Abstract

We report the first findings of several occurrences of lawsonite and metamorphic aragonite in the meta-sediments from the Combin Zone (Piemonte–Liguria ocean, Western Alps), where the early blueschist-facies episode is poorly documented. New field and metamorphic data (thermodynamic modelling and Raman spectroscopy on carbonaceous material) are used to elucidate the  $P$ – $T$  evolution and fluid composition of the Combin Zone and investigate the lawsonite growth and breakdown reactions. Two tectonometamorphic units have been identified within the Combin Zone with distinct geometry, lithological content and  $P$ – $T$  conditions. In the higher grade unit, metamorphic aragonite occurs as inclusions in titanite. Lawsonite and garnet were stable at peak  $P$ – $T$  conditions ( $\sim 16$ – $17$  kbar and  $460$ – $480$  °C) at very low  $X(\text{CO}_2)$  values. Lawsonite is systematically pseudomorphed, but preserves hourglass zoning or internal fabric associated with the prograde ductile deformation. The lower grade unit ( $\sim 8 \pm 1$  kbar  $\sim 370$ – $400$  °C) is discontinuously exposed along the western base of the continental Dent Blanche nappe and records  $P$ – $T$  conditions similar to those recorded by the Dent Blanche nappe. A metamorphic discontinuity is, therefore, documented between the largest part of the Combin Zone on the one hand, and the Dent Blanche nappe on the other hand. The discovery of lawsonite and metamorphic aragonite allows a better understanding of the large-scale metamorphic structure of the Western Alps.

**Keywords** Lawsonite · Aragonite · Subduction · Combin · Piemonte–Liguria Ocean

## Introduction

Lawsonite  $\text{CaAl}_2\text{Si}_2\text{O}_7(\text{OH})_2 \cdot \text{H}_2\text{O}$  and aragonite (the orthorhombic polymorph of  $\text{CaCO}_3$ ) are diagnostic minerals of low-temperature–high-pressure conditions, as experimentally established since the 1960s (lawsonite: Newton and Kennedy 1963; Nitsch 1972; Schmidt and Poli 1994;

Schmidt 1995; aragonite: Johannes and Puhan 1971; Hacker et al. 2005).

Lawsonite has been recognized as an essential carrier of  $\text{H}_2\text{O}$  in subduction zones (Poli and Schmidt 1997; Schmidt and Poli 1998; Tsujimori and Ernst 2014; Whitney et al. 2020), and its potential for geochronology shown in several localities (e.g. Mulcahy et al. 2009; Vitale Brovarone and Herwartz 2013). In addition to specific  $P$ – $T$  conditions, lawsonite occurrence is restricted to rocks containing enough  $\text{CaO}$  and  $\text{Al}_2\text{O}_3$ , typically mafic rocks (meta-basalt and meta-gabbro), and  $\text{Ca}$ -rich sedimentary rocks like meta-greywackes, originally containing a significant proportion of volcanic clasts, and meta-marls (e.g. Fornash et al. 2019). Due to its large  $\text{H}_2\text{O}$  content (typically ca. 12 wt%), the presence of lawsonite in metabasic rocks requires a significant addition of water before the subduction metamorphism, typically by hydrothermal metamorphism following the emplacement of these magmatic rocks (Poli and Schmidt 2002; Staudigel 2014). Unlike metabasic rocks, meta-marls are initially always  $\text{H}_2\text{O}$ -saturated since their deposition and diagenesis on top of the oceanic crust.

Communicated by Hans Keppler.

✉ Paola Manzotti  
paola.manzotti@geo.su.se

<sup>1</sup> Department of Geological Sciences, Stockholm University, 106 91 Stockholm, Sweden

<sup>2</sup> Univ Rennes, CNRS, Géosciences Rennes-UMR 6118, 35000 Rennes, France

<sup>3</sup> Česká Geologická služba, Prague 1, Czech Republic

<sup>4</sup> Laboratoire Magmas et Volcans, Université Clermont Auvergne, CNRS, IRD, OPGC, 63000 Clermont-Ferrand, France

The distribution and preservation of lawsonite at the scale of a subduction/collision belt reflects, therefore, (i) the occurrence of favourable bulk-rock chemical compositions, (ii) the pressure–temperature ( $P$ – $T$ ) paths followed by the different rocks/units and (iii) the fluid history of the rocks under consideration (e.g. Guitard and Saliot 1970; Clarke et al. 2006). Lawsonite may occur as a prograde to peak mineral in  $H_2O$ -rich rocks, and its preservation is favoured by cooling during decompression. Isothermal decompression is associated in most cases with the breakdown of lawsonite, which is replaced by various assemblages of chlorite, muscovite, paragonite and epidote/zoisite (e.g. Felix and Fransolet 1972; Ballèvre et al. 2003; Schumacher et al. 2008; Hamelin et al. 2018). Even in rocks that have initially an unfavourable bulk chemical composition (lack of Ca, Al and  $H_2O$ ), lawsonite may also develop, provided fluid access significantly changes the bulk chemistry of the system (e.g. Martin et al. 2011; Vitale Brovarone et al. 2014a, 2020; Vitale Brovarone and Beyssac 2014).

Metamorphic aragonite is much rarer than lawsonite, although carbonate-bearing rocks are quite common in blueschist- and eclogite-facies terrains. Metamorphic aragonite is well preserved in some blueschist-facies rocks (California: Coleman and Lee 1962; McKee 1962; Ernst 1965, Washington State: Vance 1968; Evans and Misch 1976; Crete: Seidel 1977; Theye and Seidel 1993, Turkey: Cogulu 1967; Okay 1982; Topuz et al. 2006; Topuz and Okay 2014), but absent or very sparsely reported in most other belts. This is generally attributed to the fast kinetics of the aragonite to calcite transformation (Brown et al. 1962; Carlson and Rosenfeld 1981; Hacker et al. 2005).

In this paper, we report new occurrences of lawsonite in the Western Alps, in an area where this mineral was—surprisingly—never reported, although most authors assumed the existence of a blueschist-facies metamorphism, albeit very poorly documented, in that region. In addition to this paradoxical situation, we report, from the same samples, the third finding of metamorphic aragonite in the European Alps. We then constrain the  $P$ – $T$  path and fluid composition of these rocks, and compare it with other blueschist-facies units of the Western Alps. We are, therefore, in a position to better constrain the large-scale metamorphic zonation of the Western Alps, and solve the paradox of the lawsonite distribution.

## Geological setting

The Alps result from the collision of the European and Adriatic plates after the subduction of the Piemonte–Liguria Ocean, a slow-spreading small oceanic domain (Manzotti et al. 2014a; McCarthy et al. 2020; Le Breton et al. 2021)

of Jurassic age (e.g. De Wever and Caby 1981; Lombardo et al. 2002; Kaczmarek et al. 2008; Decrausaz et al. 2021).

## Lawsonite distribution in the Western Alps

As a general rule, lawsonite (or pseudomorphs after lawsonite) frequently occurs in the ocean-derived units and in the Mesozoic covers of the continent-derived units (e.g. Ellenberger 1960; Michard 1967; Goffé and Chopin 1986; Bousquet et al. 2004). Some lawsonite may be found in Permian meta-andesites (Saliot 1973; Houfflain and Caby 1987; Schwartz et al. 2000; Ballèvre et al. 2020). Lawsonite is very rare or lacking in units made of reworked (polycyclic) Palaeozoic basement (e.g. Pognante 1989). This primarily reflects the control of the bulk-rock chemical composition (including the availability of  $H_2O$ ) on lawsonite development.

Overall, in the Western Alps, the oceanic units may be divided into two main types (e.g. Agard 2021), i.e. those dominated by sediments with few ophiolite complexes (called S-type units), and those largely made of serpentinites (formerly exhumed mantle) associated with meta-gabbros and meta-basalts, with no or restricted occurrences of sediments (referred to as MUM-type units). A metamorphic difference is associated with this lithological distinction (Fig. 1): the S-type units display low-grade blueschist-facies parageneses, whereas the MUM-type units are characterized by high-grade blueschist- and eclogite-facies parageneses (e.g. Bousquet et al. 2012; Agard 2021). The S-type units are generally considered as recording tectonic processes in an accretionary prism, while the MUM-type units would represent the material of the downgoing oceanic slab (e.g. Marthaler and Stampfli 1989; Vitale Brovarone et al. 2014b; Agard 2021).

Lawsonite (or pseudomorphs after lawsonite) is widespread in metabasic rocks and calcschists of the oceanic units of both the MUM (Fry and Fyfe 1971; Bearth 1973; Dal Piaz 1974; Angiboust et al. 2009) and S type (Bearth 1962; Caron 1974; Pognante and Kienast 1987; Lefeuvre et al. 2020). In the S-type units, lawsonite tends to be largely preserved in the western part of the belt (Fig. 1), whereas it is mostly found as pseudomorphs in the eastern, more internal parts of the belt. This is attributed to increasing peak  $P$ – $T$  conditions across the Alpine belt (e.g. Michard 1967; Goffé and Chopin 1986; Agard et al. 2001; Michard et al. 2004; Gabalda et al. 2009; Plunder et al. 2012).

However, the known distribution of lawsonite in the S-type units reveals a paradox. The distribution of lawsonite has been shown on maps with increasing details (Bearth 1962; Kienast and Velde 1970; Bocquet 1971, 1974; Goffé and Chopin 1986; Goffé et al. 2004; Bousquet et al. 2004, 2008). These maps indicate that lawsonite (or pseudomorphs after lawsonite) is missing in meta-sediments in the area between the east–west trending Aosta Fault to the south and

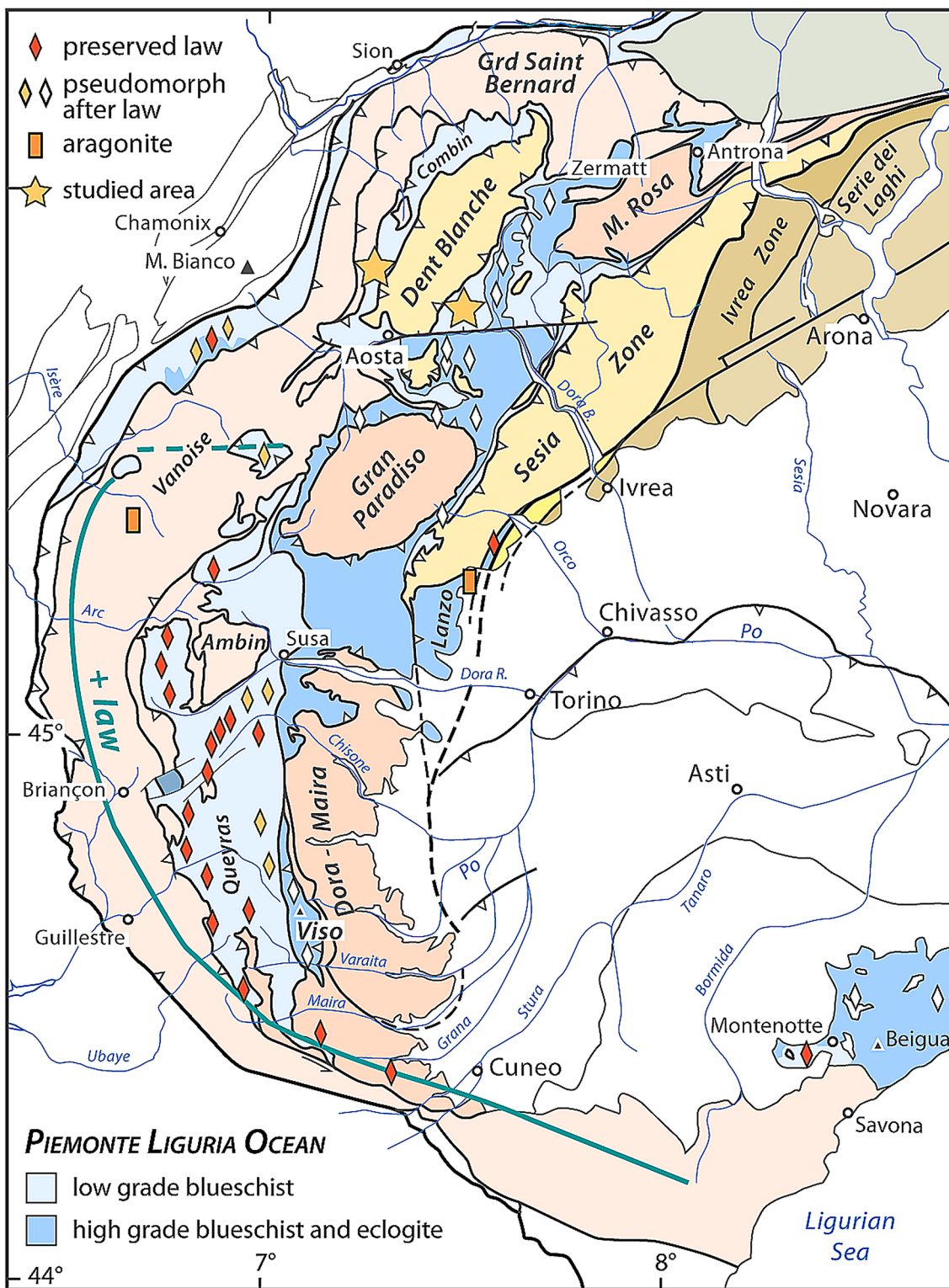


**Fig. 1** Simplified geological map of the Western Alps, redrawn after the Structural Model of Italy (Bigi et al. 1983) displaying the occurrences of preserved (red symbols) and pseudomorphed (yellow and white symbols, in low-grade blueschists and high-grade blueschists and eclogites, respectively) lawsonite within the Piemonte-Liguria Ocean (Bearth 1966; Bocquet 1971, 1974; Goffé and Chopin 1986; Bousquet et al. 2004). Note the lack of reported lawsonite in the

Combin Zone, north of the Aosta Fault. The yellow stars indicate the location of the studied areas. Note also that only two occurrences of metamorphic aragonite are reported in the Western Alps, in the Mesozoic sedimentary cover of the Briançonnais basement in the Vanoise area (Gillet and Goffé 1988) and in the Lanzo Massif (Vitale Brovarone et al. 2017; Giuntoli et al. 2020)

the Simplon Fault to the north (Fig. 1). While lawsonite is abundant in the south-western Alps (e.g. Queyras, Ubaye, Montenotte), it has never been reported from the Combin Zone, considered as an equivalent of these regions in the north-western Alps. The proposed lawsonite-glaucophane zone, or the lawsonite 'isograd' running parallel to the belt in the SW Alps, is either absent or drawn as transverse to the belt in the NW Alps (Kienast and Velde 1970; Goffé and Chopin 1986). Similarly, Agard and Lemoine (2005) have drawn three isograds running parallel to the belt in the SW Alps (namely, with increasing grade, lawsonite<sup>+</sup>, carpholite<sup>+</sup>, and chloritoid<sup>+</sup>). North of the Aosta Fault, these isograds are not identified, and are replaced by a glaucophane<sup>+</sup> isograd. This difference could suggest that the metamorphic structure of the Alpine belt changes along strike. Indeed, the metamorphic history may have been different in both areas (with peak *P–T* conditions above the lawsonite stability field in the S-type units of the NW Alps), which would have major implications for the thermal gradient along the Alpine subduction zone.

### The studied area

This study focuses on the north-western Alps, where the oceanic units derived from the Piemonte–Liguria Ocean are classically divided into two main groups on the basis of lithological, metamorphic and tectonic criteria (Kienast 1973; Dal Piaz 1974; Ernst and Dal Piaz 1978; Burri et al. 1999; Dal Piaz et al. 2015).

The Zermatt Zone is made of dismembered ophiolites dominated by mantle-derived serpentinized peridotites, meta-gabbros and meta-basalts, with subordinate meta-sediments. Because these lithologies display spectacular eclogite-facies assemblages, they attracted a large number of studies (e.g. Bearth 1967; Reynard and Ballèvre 1988; Angiboust et al. 2009; Bucher and Grapes 2009; Groppo et al. 2009; Dragovic et al. 2020; Kempf et al. 2020). The Zermatt Zone is a typical example of a MUM-type unit.

The Combin Zone is essentially made of meta-sediments, with minor, strongly dismembered, ophiolitic bodies. Several subunits may be recognized in the Combin Zone, like the Tsaté nappe (Sartori 1987), the Aiguilles Rouges d'Arolla and the Mont de l'Etoile units (Decrausaz et al. 2021). However, the metamorphic history of the Combin Zone is poorly known, and rather deceptive, because it is dominated by a greenschist-facies metamorphism. An earlier blueschist-facies episode is accepted in most syntheses (e.g. Bousquet et al. 2012; Dal Piaz et al. 2015; Agard 2021; Tajčmanová et al. 2021). However, key *HP* mineral assemblages are rarely reported, with the exception of manganese-rich minerals in meta-cherts (e.g. Baldelli et al. 1983). Rare sodic amphiboles of varying composition (magnesian riebeckite, ferro-glaucophane and glaucophane) have been

found in meta-basalts (Sperlich 1988; Martin and Cortiana 2001; Angiboust et al. 2014), although derivation of *P–T* conditions using them is strongly dependent on the Fe oxidation state (Manzotti et al. 2020). Overall, this suggests that blueschist-facies conditions have been attained in the Combin Zone. However, as emphasized by Epstein et al. (2021), neither lawsonite nor pseudomorphs after lawsonite have been reported in the Combin Zone, in stark contrast with the S-type units in the SW Alps.

Two occurrences of metamorphic aragonite have been found in the European Alps, namely in the Mesozoic cover of the External Vanoise (Gillet and Goffé 1988) and in ophicarbonates from the Lanzo Massif (Vitale Brovarone et al. 2017; Giuntoli et al. 2020). In particular, metamorphic aragonite is unknown in all other oceanic units from the Western Alps, whether they belong to the Combin-, S-type or Zermatt-, MUM-type units.

## Methods

### Mineral chemistry

Mineral analyses were performed with a Cameca SX100 electron microprobe (Microsonde Ouest, Brest, France) operating in the wavelength-dispersive mode. Operating conditions for spot analyses were set to 15 kV, 20 nA and 10 s counting time on the peak (spot size = 1 µm). The  $\phi(\rho Z)$  matrix correction was applied based on Pouchou and Pichoir (1985). Standards were natural albite (Na, Si), orthoclase (K), corundum (Al), wollastonite (Ca), forsterite (Mg), MnTiO<sub>3</sub> (Mn, Ti), andradite (Fe), Cr<sub>2</sub>O<sub>3</sub> (Cr), NiO (Ni). A JEOL JXA-8530 electron probe microanalyzer at the Institute of Earth Science of the University of Lausanne (Switzerland) was used to acquire X-ray compositional maps in wavelength-dispersive mode. Operating conditions for compositional mapping were set to 50 ms on 0.7 µm pixel, using an acceleration voltage of 15 kV and a current of 20 nA. Mineral abbreviations and symbols are those used by THERMOCALC (Holland and Powell 1998; Table S1 in the Supplementary Information). Muscovite is used hereafter for all potassic white micas, whatever the Si content. Representative analyses of selected minerals are given in Tables S2–S5 in the Supplementary Information.

### Bulk-rock chemistry

Major-element compositions of selected samples (Table S6 in the Supplementary Information) were determined in whole-rock samples by ICP–AES (CRPG, Nancy). Bulk-rock glasses were prepared by mixing appropriate proportions (1:5) of fine-grained rock powder with di-lithium tetraborate. Details about the method used for the analyses

are available in Carignan et al. (2001). The composition of two calcschist samples (OL30 and OL32) displaying pseudomorphs after lawsonite has been also measured by the area scan method using a scanning electron microscope (JSM-7100 F, University of Rennes 1). The chemical composition of areas of  $2 \times 3$  mm in size with pseudomorphs after lawsonite was analysed and averaged.

### Raman spectroscopy of inclusions in titanite

Mineral inclusions in titanite were identified using Raman micro-spectroscopy at the Laboratoire Magmas et Volcans (Clermont-Ferrand, France). The analyses were carried out in back-scattered geometry using a Renishaw InVia confocal micro-spectrometer equipped with a  $532.1 \pm 0.3$  nm diode laser, a Peltier-cooled CCD detector, a Rayleigh rejection edge filter, and a Leica DM 2500M optical microscope with a motorized XYZ stage. Daily calibration of the spectrometer was performed using a silicon standard ( $520.5 \text{ cm}^{-1}$  peak). The analyses were carried out using a grating of 2400 grooves/mm, a  $20\text{-}\mu\text{m}$  slit aperture (high confocality setting), a  $100\times$  microscope objective, and  $\sim 1$  mW laser power on the sample. These analytical conditions result in a spectral resolution of  $\sim 0.4 \text{ cm}^{-1}$ . Each analysis lasted 30 s (i.e., 3 accumulations of 10 s). The WiRE™ 4.4 software recorded the spectra in the  $\sim 90\text{--}1350 \text{ cm}^{-1}$  wavenumber range. Spectra of all host crystals (titanite) were acquired, and, if necessary, subtracted from the spectra of very small inclusions (few  $\mu\text{m}$ ) that were often contaminated by the signal coming from the host.

### Raman spectroscopy on carbonaceous material (RSCM) method

Regional metamorphic processes produce a gradual transformation of the organic matter present in rocks to CM (carbonaceous material). The peak  $T$  reached by samples can be estimated using this graphitization process; regional metamorphic  $T$  thus controls the degree of graphitization (Beysac et al. 2002, 2003). Because graphitization is considered as an irreversible process, the  $T$  estimates are not affected by metamorphic reactions associated with retrogression. Carbonaceous material was analysed in 34 samples. Raman spectra of CM in 20 samples were obtained at the Institute of Earth Sciences (University of Lausanne) with a Horiba HR Raman-FTIR spectrometer from HORIBA Scientific ( $532.15$  nm wavelength), an integrated Raman microprobe consisting of an Olympus BX41 confocal microscope coupled to an  $800\text{-mm}$  focal-length spectrograph (Tables S7 and S8 in the Supplementary information). Raman spectra of CM in 14 other samples were obtained at the Laboratoire Magmas et Volcans (Clermont-Ferrand, France) using a Renishaw InVia confocal micro-spectrometer (Table S8

in the Supplementary Information), equipped with a  $532\text{-nm}$  diode laser. Because RSCM can be affected by several analytical mismatches, we followed closely the analytical procedures described by Beysac et al. (2002, 2003). Measurements were carried out on polished thin sections using a grating of 2400 grooves/mm, a  $20\text{-}\mu\text{m}$  slit aperture (high confocality setting), a  $100\times$  microscope objective, and  $1\text{--}5$  mW laser power on the sample surface. The laser was generally focused at  $5\text{--}15 \mu\text{m}$  depth to analyze graphite that was located below different minerals and not exposed to the surface. Each analysis consisted of six or ten accumulations of 20 s each in the  $\sim 900\text{--}2000 \text{ cm}^{-1}$  wavenumber range, containing the two principal vibrations of graphite. A spectrum of the mineral phase on top of graphite (mainly calcite, quartz, albite, muscovite, and chlorite) was systematically acquired in the  $\sim 90\text{--}1350 \text{ cm}^{-1}$  wavenumber range with an acquisition time of 15 s. On each sample, we measured at least 15–20 different grains of graphite. The spectra were processed using the WiRE™ 4.4 software: first, they were truncated, then a linear baseline correction was applied in the  $1200\text{--}1800 \text{ cm}^{-1}$  spectral range, and finally curve fitting was performed. Three bands (corresponding to G, D1, and D2 components, respectively at  $\sim 1580$ ,  $\sim 1350$ , and  $\sim 1620 \text{ cm}^{-1}$ ) were generally necessary to fit the graphite spectrum; few spectra required a fourth component centered at  $1500\text{--}1520 \text{ cm}^{-1}$ . The degree of organization of CM is quantified by the relative area of the G, D1, and D2 components of CM in Raman spectra. This is equal to  $D1/(G + D1 + D2)$  and it is defined as the peak area ratio (R2 ratio).

To evaluate the inter-laboratory reproducibility and accuracy, two independent measurements were carried out on a graphite-bearing sample (OL30, Table S8 in the Supplementary Information) at both University of Lausanne and Laboratoire Magmas et Volcans and gave consistent results (calculated  $T$  of  $482 \pm 20 \text{ }^\circ\text{C}$  and  $477 \pm 12 \text{ }^\circ\text{C}$ , respectively). Another sample (VT08142, a Mesozoic meta-sediments from the Dent Blanche Tectonic System, Fig. 7) was analyzed at the University of Bern (Manzotti et al. 2014b) and at the Laboratoire Magmas et Volcans: the obtained  $T$  are consistent ( $434 \pm 7 \text{ }^\circ\text{C}$  and  $444 \pm 8 \text{ }^\circ\text{C}$ , respectively).

### Thermodynamic modelling

#### P–T pseudosections

$P$ – $T$  pseudosections were calculated in the chemical system  $\text{MnO}\text{--}\text{Na}_2\text{O}\text{--}\text{CaO}\text{--}\text{K}_2\text{O}\text{--}\text{FeO}\text{--}\text{MgO}\text{--}\text{Al}_2\text{O}_3\text{--}\text{SiO}_2\text{--}\text{H}_2\text{O}\text{--}\text{TiO}_2\text{--}\text{Fe}_2\text{O}_3$  (MnNCKFMASHTO) for a garnet micaschist. Given the pelitic character of the sample, the amount of  $\text{Fe}^{3+}$  was set to 5% of total Fe [ $X(\text{Fe}^{3+}) = \text{Fe}^{3+}/\text{Fe}_{\text{total}}$ ], an arbitrary low value. The fluid phase was fixed as pure  $\text{H}_2\text{O}$  and considered in excess. Phase diagrams were

calculated with the Theriak–Domino software (de Capitani and Brown 1987; de Capitani and Petrakakis 2010), using the internally consistent thermodynamic data set 5.5 (Holland and Powell 1998, updated November 2003).

The phases considered in the calculations, and the activity composition models are amphibole, clinopyroxene (Diener and Powell 2012), carpholite (Wei and Powell 2004), chloritoid (Mahar et al. 1997; White et al. 2000), chlorite (Le Bayon et al. 2006, based on Holland et al. 1998), white mica (Coggon and Holland 2002), plagioclase (Holland and Powell 2003), epidote (Holland and Powell 1998), magnetite (White et al. 2000), garnet, biotite, ilmenite, hematite (White et al. 2005).

### Isobaric $T$ - $X(\text{CO}_2)$ phase diagrams

Isobaric  $T$ - $X(\text{CO}_2)$  projections in the CaMASCH and CaFASCH systems were calculated using THERMOCALC 3.37 (Holland and Powell 1998) and the internally consistent thermodynamic dataset 5.5 (Holland and Powell 1998; updated November 2003). To investigate the mineral equilibria and fluid composition during the prograde evolution and at peak  $P$  conditions, pressure was fixed at 12, 14 and 16 kbar. The last value corresponds to the peak  $P$  estimated in this study for the micaschist OL38 and interpreted as the peak  $P$  reached by the Combin Zone. To understand the reactions that control the stability domains of the critical minerals and retrieve the first-order message, only mineral end-members (rather than solid solutions) were considered in the calculations: aragonite, calcite, kyanite, lawsonite, pyrophyllite, quartz, zoisite, either dolomite or ankerite and either clinocllore or daphnite. The fluid was treated as a binary  $\text{H}_2\text{O}$ - $\text{CO}_2$  solution.

### Field observations

This study focuses on two main areas in north-western Italy where the Combin Zone is exposed (Fig. 1). The first one is located between the underlying Grand Saint Bernard nappe and the overlying Dent Blanche Tectonic System in the Ollomont valley (Manzotti et al. 2017, 2020), where detailed field work was carried out in the Conca de By, in the area limited by the Ollomont village to the south and the Mont Avril (i.e. the Italian–Swiss border) to the north (Fig. 2). The second area is located to the south-east of the Dent Blanche nappe in the St Barthelemy valley (Fig. 1).

In both areas, the Combin Zone mainly consists of meta-sediments (~70%), greenschist-facies meta-basalts (~20%), meta-gabbros (~5%), and minor serpentized ultramafic rocks (~5%) (Manzotti et al. 2017; Manzotti and Ballèvre 2017). Three different types of meta-sediments have been distinguished:

- (i) Rare (<2%) whitish to silvery *quartz-rich garnet-bearing micaschists* (Fig. S1) associated with quartzites are exposed in metre-sized outcrops close to the Bivouac Rosazza (Fig. 2), along the Arête de la Bonne Mort and at the Tête Blanche de By. The micaschists contain minute (ca. 0.5 mm in diameter) garnet and pseudomorphs after sodic amphibole. They display a pervasive foliation marked by mm-thick quartz-rich layers alternating with muscovite- and chlorite-rich layers.
- (ii) Greyish to blackish carbonate-absent to carbonate-poor *phyllites* (~10%) are cropping out at the Col Cornet and at the Fenêtre de Durand (Figs. 2 and S1). They represent metamorphosed black shales, and they are sometimes alternating with cm-thick layers of calcschists. Phyllites mainly consist of very fine-grained (10–50  $\mu\text{m}$ ) quartz, muscovite, metamorphosed carbonaceous material (hereafter called graphite), albite, and chlorite. Albite is found as mm-size black porphyroblasts with graphite inclusions defining an internal schistosity. At the Col Cornet, thin mm- to cm-thick layers of meta-chert occur within phyllites (Fig. 2.5 in Manzotti and Ballèvre 2017). Meta-cherts are isoclinally folded with thickened hinges and thinner limbs, giving rise to rootless folds.
- (iii) Brownish to greyish calcareous-marly meta-sediments are largely dominant (~60%) and widespread in the Ollomont and St Barthelemy valleys. They are found as alternating relatively pure *marble* (previously limestone) and *micaschist* or *calcschist* layers (previously shale or marl, respectively) (Figs. 3a, b and S1). The thickness of the layers varies from a few centimetres to a few decimetres. *Marbles* are essentially made of calcite, with minor proportions of muscovite and chlorite. *Calcschists* mainly consist of calcite, quartz, white mica, albite, chlorite, graphite and accessory titanite, and a few sulphides. Numerous cm-scale veins containing quartz  $\pm$  calcite are observed in the calcschists from the Ollomont (e.g. Balme de Ba, Plan Debat, Lac de By, Fig. 2) and St Barthelemy valleys. A first generation of veins is parallel to the main schistosity, whereas veins of the second generation cut the main foliation at high angle. Cr-rich muscovite (fuchsite) crystals are observable in some calcschist layers (Fig. 2, see also Fig. 2.3 in Manzotti and Ballèvre 2017), suggesting the presence of detrital chromite in the sediment prior to metamorphism, and supporting a Cretaceous age for the sedimentation.

We discovered pseudomorphs after lawsonite in the brownish and greyish calcschists exposed in the By valley,

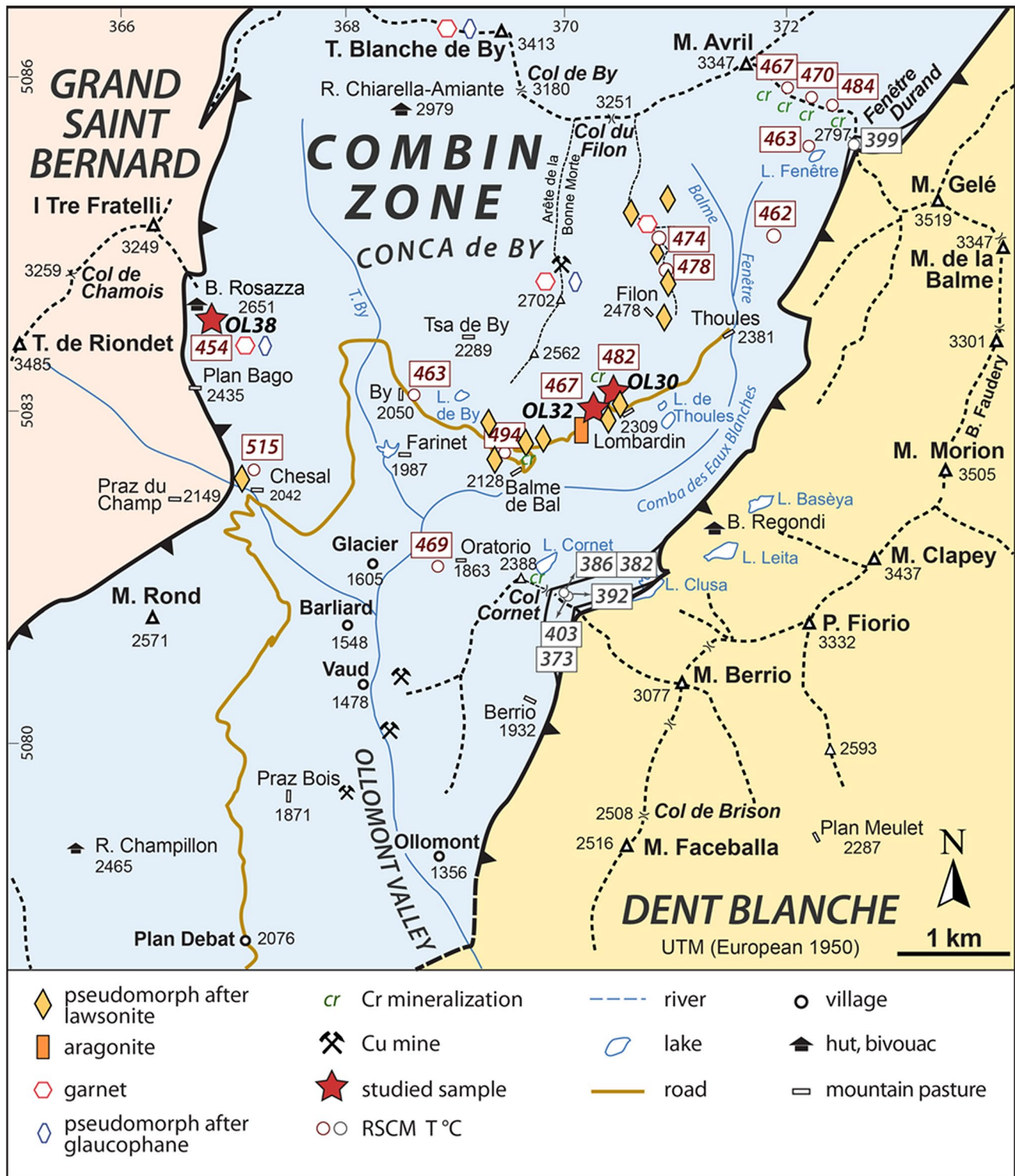


**Fig. 2** Sketch map of the studied area NW of the Dent Blanche nappe. From west to east (i.e. from the bottom to the top), the Grand Saint Bernard nappe, the Combin Zone and the Dent Blanche nappe are exposed. The Mesozoic meta-sediments and a few ophiolitic bodies of the Combin Zone are largely outcropping in the Ollomont valley. Red stars indicate the location of the studied samples. Metamorphic aragonite and pseudomorphs after lawsonite are indicated

by orange rectangle and yellow lozenges, respectively. *T* estimated in this study by RSCM are also reported. In most of the Combin Zone the RSCM temperatures are in the range ~450–500 °C (By Unit). However, a thin, discontinuous zone at the contact with the Dent Blanche nappe records lower *T* in the range ~370–400 °C (Cornet Unit)

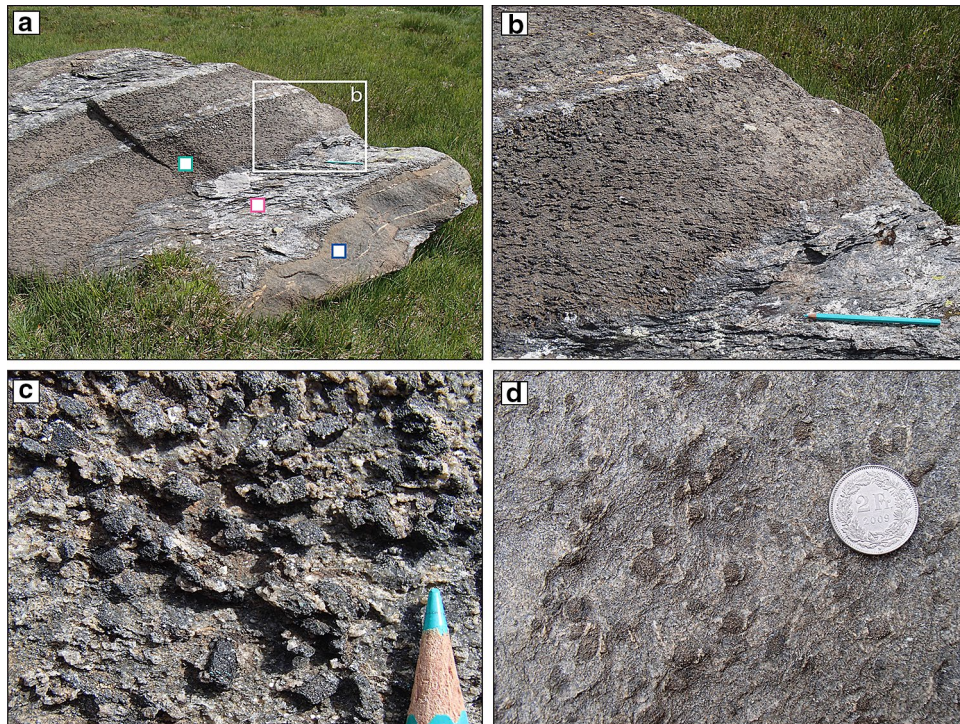


**Fig. 3** **a** Alternating layers of brownish pure marbles (meta-limestone, blue square), greyish schists (meta-shale, pink square) and brownish impure marbles (meta-marl, green square). The latter displays pseudomorphs after lawsonite. **b** Distribution of pseudomorphs after lawsonite, abundant in the phyllitic marbles and absent in the greyish schists, except in a narrow zone at the contact between the two lithologies. This field observation emphasizes how the bulk-rock

chemistry controls lawsonite development. **c** A weathered surface where dissolution of calcite has put in relief pseudomorphs after lawsonite essentially made of graphite, muscovite, paragonite, and minor calcite and therefore less soluble than the matrix. Note that some of the pseudomorphs display the characteristic shape of lawsonite (short rhombohedral prisms). **d** Brownish pseudomorphs after lawsonite

between Balme de Bal and Col du Filon (Fig. 2) as well as in the greyish calcschists cropping out in the southern St Barthelemy valley (Fig. 1). Pseudomorphs made of greyish to blackish clusters of submillimetre-sized crystals are conspicuous, because they are standing out on weathered surfaces. In some cases, the pseudomorphs have a prismatic or lozenge shape (Fig. 3c, d), reminiscent of lawsonite. Their modal amount reaches ~30%. In strongly deformed calcschists, pseudomorphs after lawsonite are flattened parallel to the main foliation (Figs. 3b and S1).

### Petrography and mineral chemistry

A detailed study of three meta-sedimentary samples from the Ollomont valley has been performed. The garnet micaschist (OL38) is a good candidate for investigating the  $P$ – $T$  evolution of the meta-sediments, whereas samples OL30 and OL32 are used to study the nature and the distribution of the pseudomorphs in the meta-sediments. In addition, the petrography and mineral chemistry of lawsonite- and garnet-bearing calcschists from the St Barthelemy valley are also described.

### Garnet micaschist OL38

Sample OL38 has been collected below the “Tre Fratelli” mountain, close to the Bivouac Rosazza at 2674 m (Fig. 2). The rock is light grey to greenish in colour (Fig. S1) and mainly consists of muscovite (30%), quartz (30%), chlorite (15%), garnet (10%), and albite (5%). Accessory rutile, ilmenite, tourmaline, epidote, and apatite are also present (Fig. S2).

Subhedral garnet porphyroblasts (up to 500  $\mu\text{m}$  in size; Fig. 4a) display a growth zoning with a significant core-to-rim decrease in spessartine (from 54 to 17 mol%), compensated by an increase of almandine (from 27 to 59 mol%). Grossular content is rather constant in the core (~17 mol%) with a slight increase (~22 mol%) in the rim (Fig. 4c). Crystals locally display a snowball structure with an internal rotated foliation ( $S_1$ ) defined by tiny inclusions of rutile and minor quartz. Tourmaline and apatite also occur as inclusions in garnet, with the latter preferentially located in the garnet core.

Garnet is mostly enveloped by the dominant foliation  $S_2$  (stage 2) (Fig. 4a), which is marked by the alternation of discontinuous mm-thick layers of Si-rich

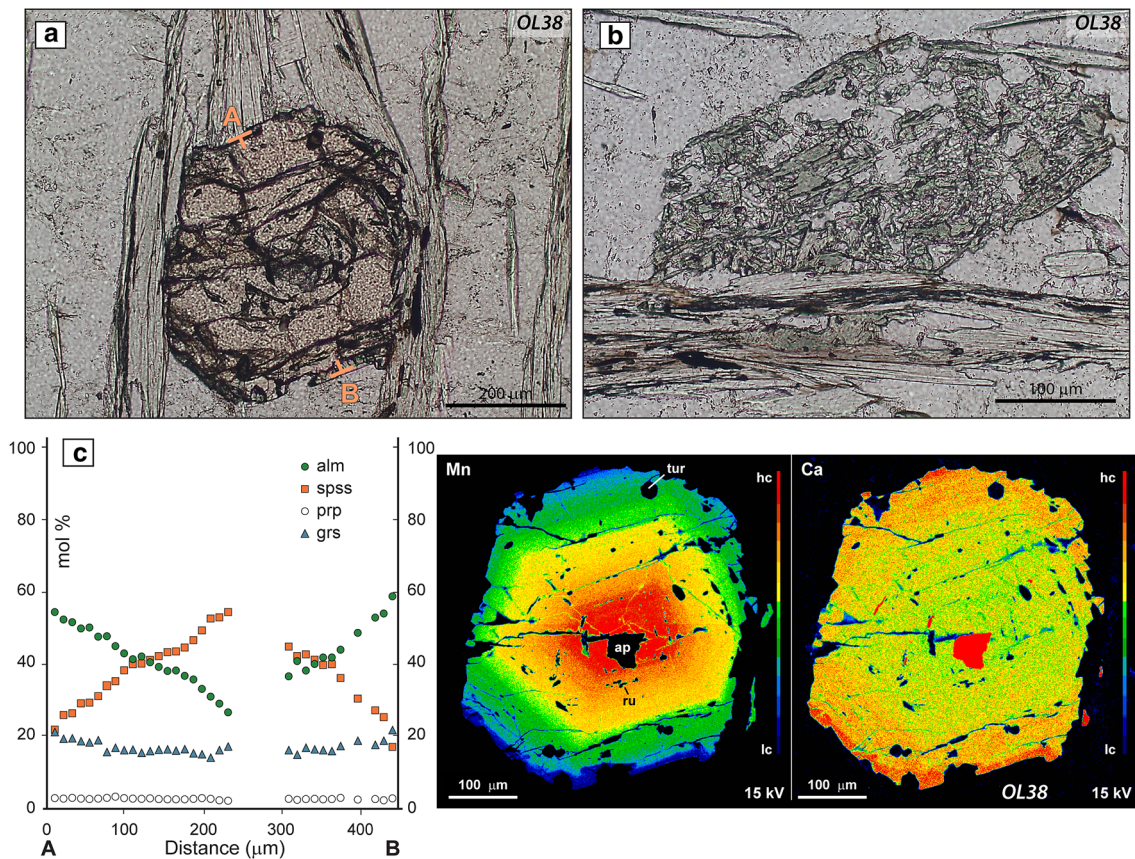


**Fig. 4** Plane polarized light thin section photomicrographs (a, b) and chemical data (c) from the garnet micaschist OL38. **a** Garnet porphyroblast wrapped by  $S_2$  foliation. **b** Pseudomorph consisting of quartz,

muscovite (Si 3.31–3.41 a.p.f.u., Fig. S2) and minor chlorite ( $X_{Mg} = 0.44–0.48$ ,  $X_{Mn} = 0.01–0.02$ ), and several millimetres thick quartz lithons. Apatite, tourmaline, and ilmenite replacing rutile, are found in the muscovite layers and oriented parallel to the main foliation  $S_2$ .

During stage 3, chlorite ( $X_{Mg} = 0.43–0.49$ ,  $X_{Mn} = 0.02–0.03$ ) locally partly replaces garnet. In addition, several minerals overgrow the  $S_2$  foliation: muscovite (Si 3.21–3.24 a.p.f.u., Fig. S2), fine-grained idiomorphs of epidote with allanitic cores, and millimetre-sized albite crystals. Lozenge-shaped pseudomorphs (Fig. 4b) are found in quartz lithons and consist of fine-grained aggregates of chlorite ( $X_{Mg} = 0.46–0.50$ ,  $X_{Mn} = 0.01–0.02$ ), quartz, locally albite, and Mn-rich ilmenite (MnO up to ~12 wt%) replacing rutile. Considering their shape and the replacement products, the pseudomorphs are attributed to sodic amphibole, similar to those described in other areas (e.g. Compagnoni 1977).

In summary, it is interpreted that the main mineral assemblage comprises garnet, chlorite, muscovite, rutile, quartz and probably glaucophane. Garnet texture and growth zoning reflect syntectonic crystallisation along a prograde  $P–T$  path. Albite, epidote, muscovite, chlorite

chlorite and albite, resulting from the breakdown of a sodic amphibole. **c** Compositional profile of garnet, along the line A–B and X-ray maps for Mn and Ca (*hc* high concentration; *lc* low concentration)

and the minerals pseudomorphing glaucophane, interpreted as retrograde phases, crystallised subsequently.

### Calcschists with pseudomorphs after lawsonite

Meta-sediments from the Combin Zone display a large range of compositions, from metapelites (micaschists without calcite) to meta-limestones (almost pure marbles with very minor mica), with all compositional intermediates (phyllitic marbles and calcschists). This difference reflects the sedimentary layering, with alternating layers a few cm to a few dm thick (Fig. 3a). At first sight, the distribution of the pseudomorphs is highly heterogeneous, because they are absent in the marbles and the micaschists, and may be abundant in the interbedded calcschists (Fig. 3a, b). This clearly reflects a bulk-rock control on the modal abundance of the pseudomorphed phase (see below the discussion on the bulk-rock chemistry). Besides this control by the original sedimentary character, two types of pseudomorph-bearing calcschists have been distinguished and are described below.

### Calcschist with graphite-rich pseudomorphs after lawsonite (OL30)

Sample OL30 is a brownish calcschist (Fig. 5) collected from a 15-cm-thick layer interbedded with pure marble layers (~10-cm thick). In the field, the alternation of calcschist and pure marble layers is parallel or slightly oblique to the main regional foliation (Fig. S1). A mm-thick layering ( $S_0$ ) is deformed by irregularly spaced crenulations ( $S_1$ ). The layering is defined by discontinuous ~1 to 2-mm-thick whitish and brownish domains (Fig. 5a). The whitish domains comprise inclusion-free calcite ( $\text{FeO} = 0.07\text{--}0.09$  wt%,  $\text{MgO} = 0.24\text{--}0.26$  wt%), minor quartz and white mica. In the brownish domains, calcite is Fe-richer ( $\text{FeO} = 0.44\text{--}1.38$  wt%,  $\text{MgO} = 0.18\text{--}0.75$  wt%) and typically cloudy, because riddled with inclusions of iron oxides and minor rutile. The domains with or without inclusions are independent of the actual grain boundaries, suggesting that prior to the final recrystallisation the brownish domains possibly

contained ankerite–dolomite in addition to calcite. The calcite matrix shows dispersed crystals of Si-rich muscovite ( $\text{Si} = 3.17\text{--}3.38$  a.p.f.u.;  $X_{\text{Mg}} = 0.61\text{--}0.80$ , Fig. S2) and paragonite ( $X_{\text{Na}} = 0.86\text{--}0.97$ ). Graphite occurs as minute inclusions in matrix white mica, locally concentrated in the core of the crystals.

Aggregates (up to 1 cm in size) with a characteristic lozenge section (Fig. 5b) contain muscovite ( $\text{Si} = 3.13\text{--}3.23$  a.p.f.u.;  $X_{\text{Mg}} = 0.73\text{--}0.79$ ), paragonite ( $X_{\text{Na}} = 0.83\text{--}0.97$ ), graphite and minor fine-grained calcite, quartz, and rare apatite and allanite.

Polished surfaces of the calcschists reveal spectacular sector zoning in the pseudomorphs (Fig. 5). The hourglass textures also correspond to a chemical sector distribution, as reported both in fresh (e.g. Ueno 1999; Tsujimori and Ernst 2014; Vitale Brovarone et al. 2014a; Fornash et al. 2019; Lefeuvre et al. 2020) and pseudomorphed lawsonite (Philippon et al. 2013; López-Carmona et al. 2014). Specifically, Ti is preferentially concentrated in sectors opposite to those

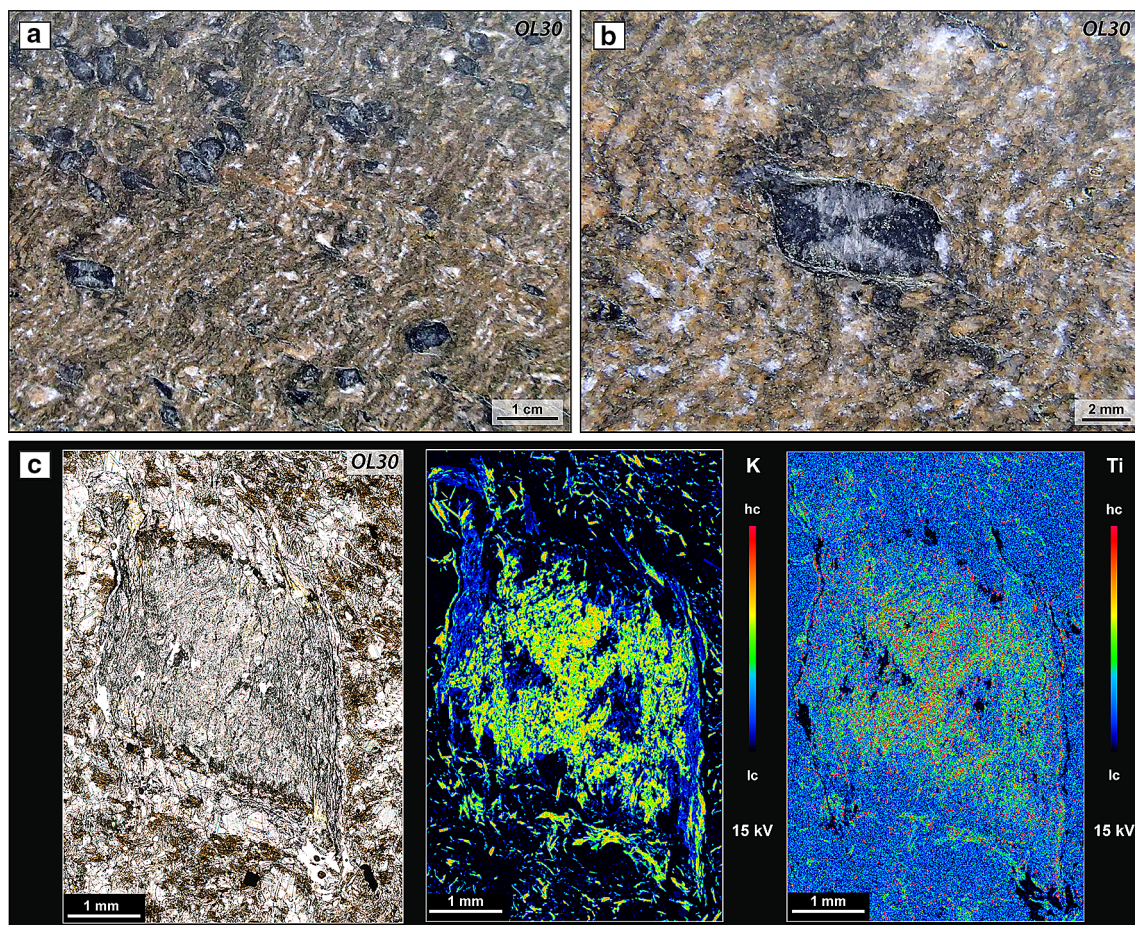


**Fig. 5** Hand sample and microscopic aspect of brownish calcschist containing pseudomorphs after lawsonite (sample OL30). **a** Polished surface displaying spectacular sector-zoned pseudomorphs after lawsonite, overgrowing a crenulated layering. **b** Detail of a pseudomorph

displaying an hourglass distribution of graphite inclusions. **c** Photomicrograph and X-ray map for K and Ti of a pseudomorph after lawsonite showing the characteristic sector zoning

with preferential incorporation of graphite (Fig. 5). Sector zoning in itself is not diagnostic of lawsonite, and may be observed in many other metamorphic minerals (e.g. chloritoid, staurolite, andalusite, garnet, diopside/omphacite, ...). However, given (i) the consistency of their orthorhombic shapes (which excludes garnet), (ii) the nature of the breakdown products, and their similarity to those found in partial pseudomorphs observed in similar rocks from the Western Alps (e.g. Caron 1974; Lefeuvre et al. 2020), and (iii) their occurrence in Jurassic or Cretaceous (hence monocyclic) meta-sediments, which exclude some potential precursors like andalusite or diopside/omphacite, the aggregates are confidently interpreted as pseudomorphs after lawsonite.

Pseudomorphs after lawsonite are euhedral and mostly parallel to the axial planes of the crenulation ( $S_1$ ). Pseudomorphs after lawsonite are bounded by paragonite layers on the two opposite sides parallel to the  $S_1$ , and are surrounded by large crystals of sparry calcite on the two sides perpendicular to  $S_1$ . Mg-chlorite ( $X_{Mg} = 0.61\text{--}0.62$ ;  $X_{Mn} < 0.01$ ) is frequently found along the four edges of the lozenges.

#### Calcschist with graphite-poor pseudomorphs after lawsonite (OL32)

Sample OL32 is a greyish calcschist with a discontinuous, spaced foliation ( $S_2$ ) marked by the shape preferred orientation of Si-rich muscovite (Si 3.42–3.48 a.p.f.u.;  $X_{Mg} = 0.56\text{--}0.65$ , Fig. S2), chlorite ( $X_{Mg} = 0.49\text{--}0.51$ ;  $X_{Mn} < 0.01$ ), and graphite (Fig. 6a). Graphite is mainly concentrated in the  $S_2$  planes. Microlithons between the  $S_2$  planes display a relict foliation ( $S_1$ ) oriented at high angle to the main foliation  $S_2$ , and defined by graphite, muscovite, titanite, with dispersed grains of quartz in a matrix of calcite. Cloudy, lozenge-shaped pseudomorphs (up to 0.5 mm) are dispersed in the calcite matrix (Fig. 6b), and are generally parallel to  $S_1$ . The pseudomorphs are made of calcite containing a large amount of minute oxides. They may derive from a calcic (tremolite) or sodic (glaucophane) amphibole.

Aggregates (up to 1 cm in size) with an orthorhombic shape and containing unoriented crystals of calcite, albite, quartz, inclusion-free Si-rich muscovite (Si = 3.28–3.39 a.p.f.u.;  $X_{Mg} = 0.51\text{--}0.74$ ), and titanite are wrapped by the  $S_2$  foliation (Fig. 6a), with calcite-rich pressure shadows. Because of their characteristic shapes, they are interpreted as pseudomorphs after lawsonite. In the pseudomorphs, albite and calcite are cloudy due to the presence of tiny graphite inclusions.

Titanite (up to 0.5 mm in size;  $Al_2O_3 = 2.93\text{--}3.39$  wt%) in the pseudomorphs and in the matrix displays abundant elongated or rounded inclusions of carbonates (aragonite, calcite, dolomite-ankerite), quartz, Si-rich muscovite, pyrite, and apatite. The shape of the inclusions may record the fine-grained foliation  $S_1$  (Fig. 6c, d). Aragonite occurs as rounded

or slightly elongate inclusions (up to 10  $\mu\text{m}$  in size) in the core as well as in the rim of titanite. No cracks are present around the aragonite inclusions.

#### Lawsonite and garnet calcschists from the St Barthelemy valley

Samples VB13, VB17, VB19 are calcschists and VB21 is a phyllitic marble, all collected in the St Barthelemy valley (Fig. S3).

Sample VB13 is a typical calcschist distinguished by the occurrence of cm-sized blackish clusters moulded by the main chlorite- and white mica-bearing foliation  $S_2$ . The clusters are made of calcite and albite aggregates overgrowing an earlier foliation ( $S_1$ ) defined by elongated trails of graphite and titanite, and at high angle with respect to  $S_2$ . The clusters are interpreted as pseudomorphs after lawsonite.

Samples VB17 and VB19 contain equal amounts of quartz, carbonate, chlorite and white mica, and are distinguished from the other calcschists by the presence of albite and garnet porphyroblasts. The latter deserves some attention, because garnet is exceedingly rare in the Combin calcschists. Garnet crystals display honeycomb textures, with narrow lines of garnet separating large, rounded grains of calcite and/or quartz (Fig. S3). Calcite and quartz have different orientations from one inclusion to the other, and are typically undeformed, although they may display some undulose extinction or minor recrystallisation along their margins when in contact with the matrix foliation. The matrix foliation wraps around the garnet porphyroblasts. These textures are very similar to those described by Hawkins et al. (2007) and Okamoto et al. (2017) in micaschists and calcschists of similar metamorphic grade as the ones studied here. Overall, the modal proportion of garnet in samples VB17 and VB19 is very small (three to five ‘grains’ per thin section, each grain being about 1 mm in diameter, meaning a modal proportion less than 1 vol. %). Garnet is spessartine- and grossular-rich and poor in pyrope (spss = 26–38 mol%, grs = 18–28 mol%, alm = 34–42 mol%, prp = 2–3 mol%; Fig. S3), similar to blueschist-facies garnet-bearing marbles from the Queyras (e.g. Ballèvre and Lagabrielle 1994).

Sample VB21 comprises calcite with minor amounts of quartz and white mica, the latter defining the main foliation. Millimetre-sized dark clots are made of aggregates of calcite and minor zoisite, the latter being only found in these aggregates. The clots are wrapped by the main foliation  $S_2$  and generally contain a large amount of graphitic material, locally clearly displaying a relict straight or sigmoidal schistosity ( $S_1$ ) at high angle to  $S_2$ . This suggests that the clots derive from syn- $S_1$  porphyroblasts, replaced by calcite and zoisite during or after  $D_2$ . They are interpreted as former crystals of lawsonite.

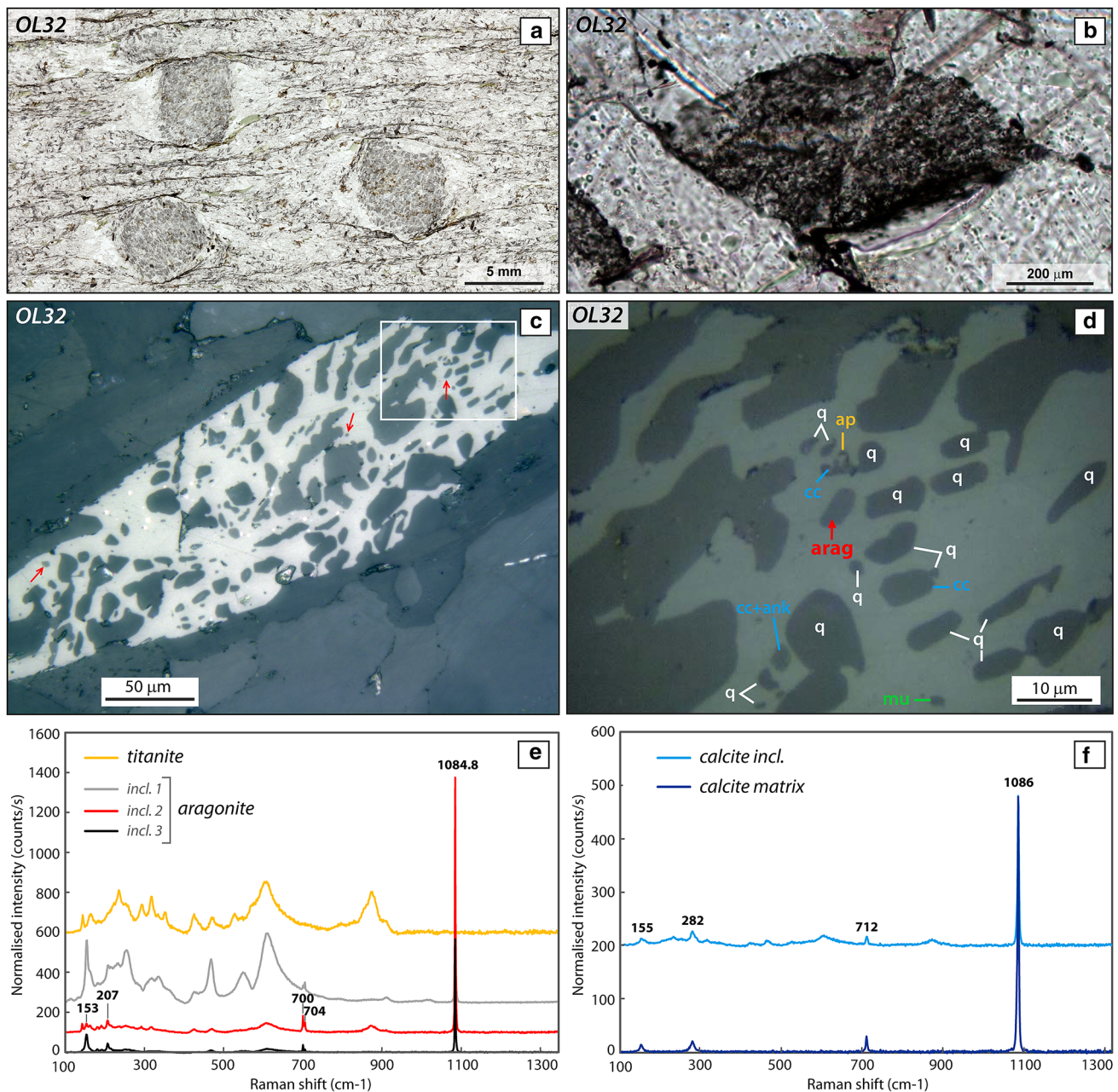


**Fig. 6** **a** Photomicrographs (plane-polarised light) of a calcschist displaying pseudomorphs after lawsonite (sample OL32). Crenulation cleavage  $S_2$ , overprinting a faint pervasive foliation  $S_1$ , is moulding the pseudomorphs, with development of calcite-rich strain shadows. **b** An example of the small-sized, lozenge-shaped pseudomorph dispersed within the recrystallized calcite matrix, and interpreted as representing former (calcic or sodic) amphibole. **c** and **d** An example of

a titanite crystal displaying numerous inclusions of carbonates (aragonite, calcite, ankerite-dolomite), quartz, Si-rich muscovite, pyrite, and apatite. The red arrows indicate three metamorphic aragonite crystals. The white rectangle is shown with a larger magnification in **(d)**. **e** Raman spectra of metamorphic aragonite included in titanite and the host titanite. **f** Raman spectra of calcite analysed in the matrix and as inclusion in titanite

## RSCM temperatures in the Combin Zone

RSCM temperatures were estimated on 34 samples (calcschists, phyllites, and garnet-micaschists) collected in the Ollomont and St Barthelemy valleys. The results are

summarised in Tables S7, S8 and S9 and shown on Figs. 2, 7.  $T$  estimates may be grouped into two subsets.

Close to the contact with the Dent Blanche nappe (Col Cornet and Fenêtre de Durand areas), four blackish phyllites and two brownish calcschists show homogeneous, relatively low temperatures in the range 373–403 °C (Figs. 2,

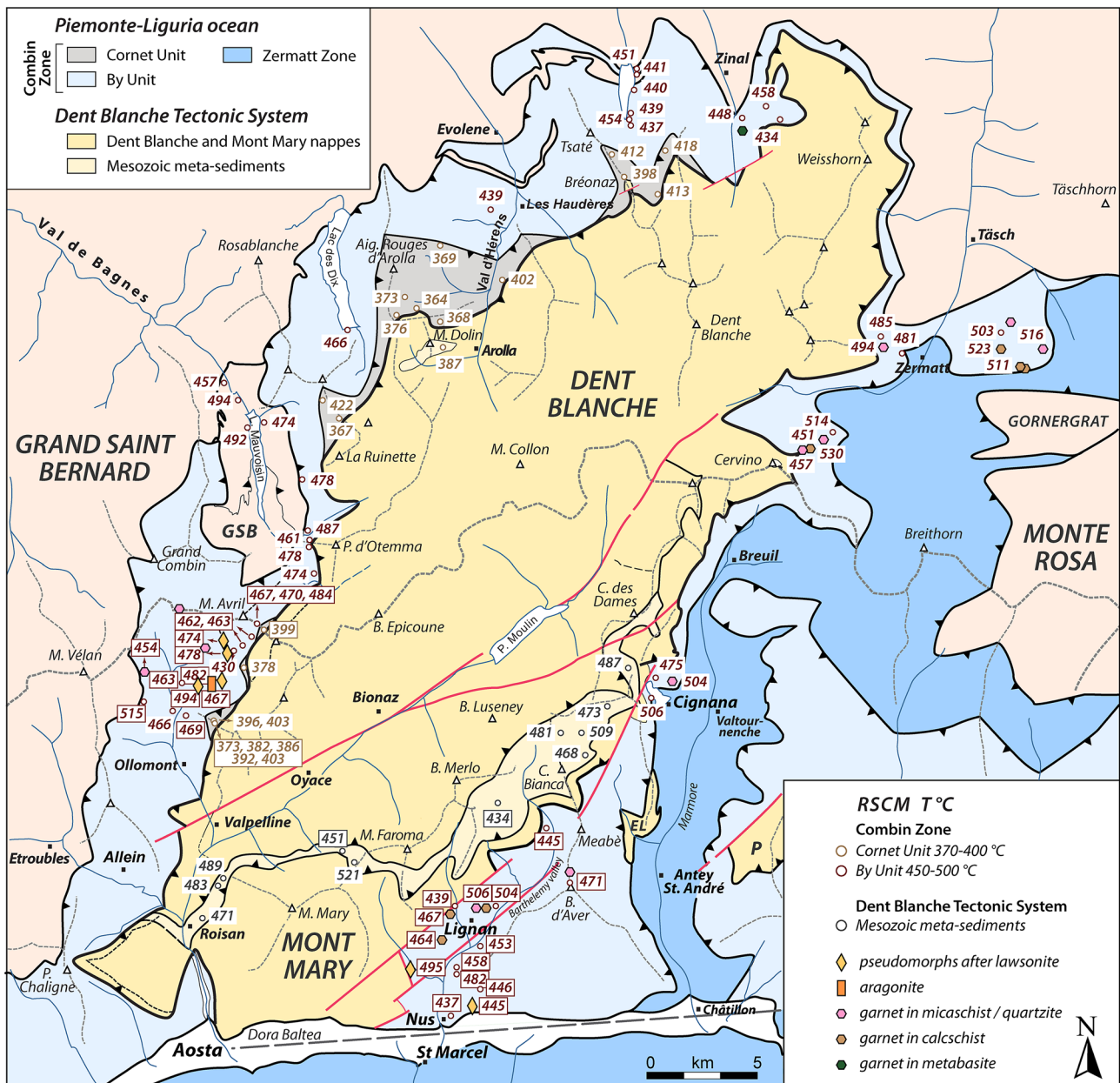


**Fig. 7** Simplified tectonic map of the studied area in the north-western Alps. The distribution of some key minerals (garnet and lawsonite), first described in this study, is indicated. In addition, RSCM data from this study are shown within rectangles (mean values of up to 20 measurements per studied sample are given in °C). These are

consistent with RSCM values taken from the literature (Negro et al. 2013; Angiboust et al. 2014; Manzotti et al. 2014b; Decrausaz et al. 2021), here shown in rectangles without contours. Note also that garnet and lawsonite occurrences have only been found in the higher  $T$  (450–500 °C) domain. *P* Pillonet; *EL* Etirol-Levaz

7). Graphite yields rather constant  $R_2$  values ranging from 0.48 to 0.65.

Higher temperatures, in the range 462–494 °C, are estimated from twelve meta-sediments (calcschists and micaschists) collected in the Ollomont valley. Graphite for the twelve samples yields constant  $R_2$  values in the range 0.21–0.48, lower than those measured in the samples collected close to the contact with the Dent Blanche nappe.

Only one sample, namely the calcschist OL51, sampled close to the contact with the Grand Saint Bernard Unit in the Chesal area, displays a slightly higher  $T$  of ~515 °C ( $R_2 = 0.21$ –0.37). According to the acquired data, the temperature distribution is rather homogeneous within each zone (i.e. 373–403 °C and 462–494 °C, respectively). The samples used for detailed petrological investigations belong to the higher  $T$  subset. The garnet micaschist (OL38) contains

very rare graphite crystals yielding a  $T$  of  $457 \pm 21$  °C (Figs. 2, 7). The lawsonite-bearing calcschists OL30 and OL32 yield a RSCM  $T$  of  $482 \pm 20$  °C and  $467 \pm 28$  °C, respectively.

Fourteen calcschist samples from the St Barthelemy valley yielded similar  $T$  values in the range 440–500 °C ( $R2=0.23$ – $0.49$ ). As in the north-west of the Dent Blanche nappe, no systematic  $T$  differences can be observed between the samples (Table S9). The two garnet-bearing calcschists and the two lawsonite-bearing calcschists have provided  $T$  values of  $467 \pm 30$  °C ( $R2=0.29$ – $0.46$ ),  $506 \pm 17$  °C ( $R2=0.24$ – $0.39$ ),  $445 \pm 17$  °C ( $R2=0.34$ – $0.49$ ),  $495 \pm 23$  °C ( $R2=0.23$ – $0.40$ ), respectively.

## Whole-rock geochemistry

### Micaschists (metapelites)

Because the Piemonte–Liguria meta-sediments equilibrated at low-grade blueschist ( $T < 450$  °C) or high-grade blueschist and eclogite ( $T > 450$  °C) conditions, two schematic compatibility diagrams have been drawn (Fig. 8a, b). In the low-grade blueschist-facies, carpholite and/or chloritoid may be stable. Garnet is not stable, except when stabilized by Mn, like in the meta-cherts. In the AK(FM) projection, the micaschist OL38 (red star in Fig. 8a) shows lower  $Al_2O_3$  compared with the average pelite compositions (Shaw 1956; Mahar et al. 1997; Tinkham et al. 2001) and Piemonte–Liguria meta-pelites taken from the literature (see caption of Fig. 8), and plots close to the muscovite–chlorite tie-line. The highly aluminous Piemonte–Liguria metapelites display carpholite and chloritoid. The relatively high MnO content (0.28%) of sample OL38 results in stabilizing a spessartine-rich garnet at relatively low  $T$  (see below). With increasing  $T$  (i.e. in the high-grade blueschist and eclogite-facies), almandine–pyrope garnet becomes stable in pelitic compositions (Fig. 8b).

### Calcschists (meta-marls)

In the Combin Zone, calcschists are layered meta-sedimentary rocks with a large range of compositions resulting from mixing of a carbonate component (i.e. limestone) with a pelitic component (i.e. shale of various  $Al_2O_3$  contents). The sedimentary layering is still recognizable in all outcrops (Fig. 3a). For instance, Fig. 3a displays a characteristic field example, where brownish pure marbles (meta-limestone, blue square) are interbedded with greyish micaschists (meta-shale, pink square) and brownish impure marbles (marly meta-limestone or meta-marl, green square).

Of major interest for our purpose is the distribution of pseudomorphs after lawsonite with respect to the layering

and schistosity (Fig. 3b). The pseudomorphs are lacking in the pure marble layer (blue square) as well as in the micaschist (pink square). In contrast, they are abundant in the brownish impure marble (green square) (Fig. 3a, b) and at the contact between the greyish micaschist and the brownish pure marble, where they are concentrated in a 1–2-cm-thick layer. The modal proportions of lawsonite may vary in a single bed, like in the brownish impure marble on top of the outcrop (Fig. 3a), the modal variations of lawsonite defining internal layers inside the impure marble bed.

The above field observations reflect directly the relation between the composition of the rocks and that of lawsonite, which necessitates both Al and Ca for its growth. This may be rationalized using an ACF projection (Fig. 8c, d). The range of chemical compositions in the studied meta-sediments is represented based on (i) their Ca content (from a pure limestone to a pure shale), and (ii) mixing lines between a pure limestone and four shales with increasing  $Al_2O_3$  content (red to yellow lines in Fig. 8d). Consider three hypothetical bulk compositions representative of the three different meta-sedimentary layers shown by our reference outcrop (Fig. 3a). Neither a pure limestone (blue square) nor a pure shale (pink square) can contain lawsonite. In contrast, all intermediate bulk compositions (resulting from the mixing of a carbonate component with aluminous shales), like the brownish impure marble (green square), are favourable for the growth of lawsonite under appropriate  $P$ – $T$  conditions.

In such rocks, the lawsonite modal proportions are depicted in Fig. 8d as thin dashed lines. Along each mixing line between a pure limestone and the various shales, the largest amount of lawsonite is predicted in rocks plotting along the lawsonite–chlorite tie-line, the lawsonite modal amount increasing from 0% to more than 50% (Fig. 8d). This rationale may be used to understand the field observations.

Lawsonite is absent in pure marbles and pure shales because of the lack of an appropriate component (Al and Ca, respectively). Varying amounts of lawsonite reveal subtle differences of the bulk chemical composition between or inside marly beds, preserving and emphasizing the sedimentary bedding in a system that can be considered, to first order, as isochemical. The large amount of lawsonite at the contact between the greyish micaschist and the brownish pure marble may be interpreted in two ways. It can correspond to a thin marly layer deposited at the transition between a carbonate- and a clay-dominated sedimentation. It may also result from pre-metamorphic processes, an originally sharp transition between shale and limestone being obscured by syn-depositional bioturbation and/or early diagenesis. Alternatively, the lawsonite-rich layer may be the result of metasomatism due to localized fluid flow, with exchange of Ca and Al.

Reporting measured bulk compositions in the ACF diagram gives also some relevant information. First, the three

## Piemonte-Liguria meta-sediments

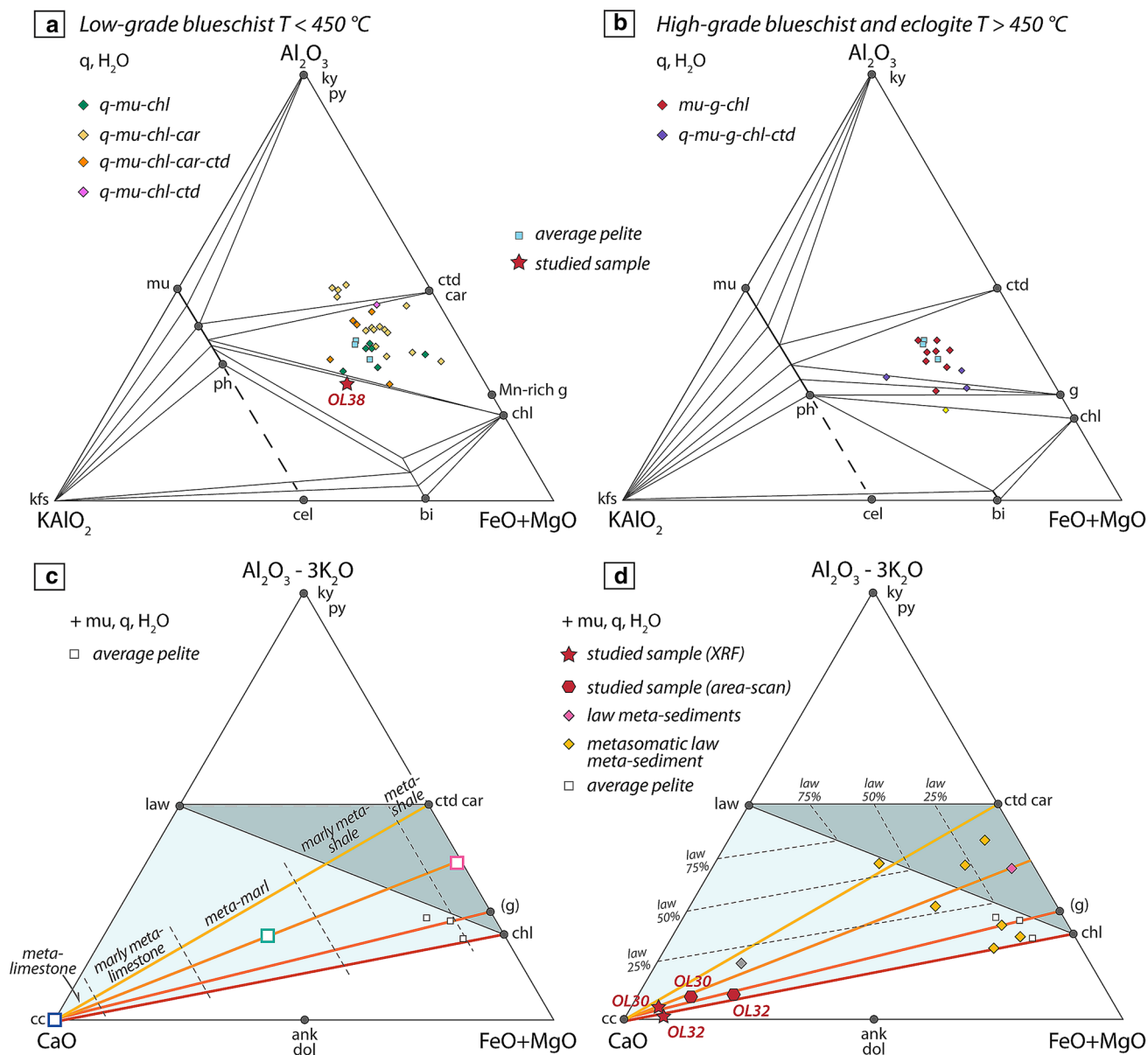


**Fig. 8** **a, b** AKF [ $\text{Al}_2\text{O}_3\text{--KAlO}_2\text{--(FeO+MgO)}$ ] diagrams projected from quartz and  $\text{H}_2\text{O}$ , showing the bulk-rock compositions of Piemonte–Liguria meta-sediments. The change in topology of the diagrams from low-grade blueschist (**a**) ( $T < 450\text{ }^{\circ}\text{C}$ ) to high-grade blueschist and eclogite (**b**) ( $T > 450\text{ }^{\circ}\text{C}$ ) reflects the disappearance of carpholite, the stabilization of spessartine-poor garnet, and the decrease in the tschermak substitution in both muscovite and biotite. Compositions of the studied sample (OL38) and other selected low-grade blueschist and high-grade blueschist and eclogite samples are plotted together with pelite (shale) compositions of Shaw (1956), Mahar et al. (1997) and Tinkham et al. (2001). Bulk compositions from low-grade blueschist are taken from the literature as follows (i) Queyras (Terra Nera—Est Fraiteve, Assietta, Albergian): Agard 1999, Bebout et al. 2013, Henry et al. 1996; (ii) Combin Zone: Garofalo 2012. High-grade blueschist and eclogite: (i) Queyras (Finestre): Bebout et al. 2013; (ii) Zermatt Zone (Cignana): Bebout et al. 2013, Ghignone et al. 2020a; (iii) Lago Superiore Unit: Angiboust et al. 2012; (iv) Viso Unit: Angiboust and Glodny 2020. **c, d** Bulk-

rock control on lawsonite occurrence and amount in the calcschists from the Combin Zone represented in ACF [ $(\text{Al}_2\text{O}_3\text{--}3\text{K}_2\text{O})\text{--CaO--(FeO+MgO)}$ ] diagram projected from quartz, muscovite, and  $\text{H}_2\text{O}$ . The large range of compositions of the calcschists results from the mixing of a carbonate component (limestone) with a pelitic component (shales of various  $\text{Al}_2\text{O}_3$  content). Modal amount of lawsonite is a function of the bulk composition of a rock. The red to yellow lines represent mixing lines between a limestone and shales of increasing  $\text{Al}_2\text{O}_3$  contents (from red to yellow). Three hypothetical bulk compositions (coloured squares in (c), see Fig. 3a) are representative of three different meta-sedimentary layers. The ACF diagram in (d) shows the bulk rock compositions of the studied meta-sediments (red symbols). Compositions of other selected samples of lawsonite-bearing meta-sediments (Queyras, Bebout et al. 2013) and metasomatic lawsonite-bearing meta-sediments (Corsica, Vitale Brovarone et al. 2014a, 2020) from the Piemonte–Liguria ocean and average pelite compositions of Shaw (1956), Mahar et al. (1997), Tinkham et al. (2001) are plotted for comparison

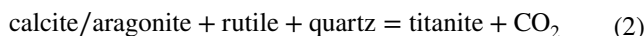


of a sodic amphibole is consistent with the pseudomorphs observed (Fig. 4b). In this field, the modelled Si content in muscovite reaches 3.35–3.38 a.p.f.u., consistent with the values measured in the studied sample. The measured rimward decrease of spessartine and increase of almandine, and the position of the garnet isopleths point towards a prograde growth of garnet. This is also compatible with the observed constant or only slightly rimward increasing amount of grossular.

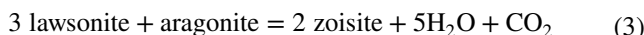
To estimate the peak conditions reached by the sample (corresponding to the end of garnet growth), the strong fractionation of manganese in garnet has been taken into account and a second pseudosection has been calculated after having subtracted the garnet cores from the bulk-rock composition (Fig. 9b). The corresponding garnet–muscovite–chlorite–amphibole–quartz–rutile stability field spans ~14–17.5 kbar and ~445–500 °C. The presence of garnet provides a lower bound to minimum *P*, whereas the chloritoid-in line sets the upper pressure limit. Peak conditions inferred from the garnet rim composition (alm = 54–59 mol%, spss = 17–22 mol%, grs = 21–22 mol%) are ~16–17 kbar and ~460–480 °C. The Si content of muscovite modelled in this field is of the order of 3.32–3.33 a.p.f.u., the lower range of the measured values. The inferred peak temperature is in agreement with the maximum *T* of 457 ± 21 °C (Table S8) calculated for this sample using the RSCM method (see above).

### T–X(CO<sub>2</sub>) projections

To investigate the stability of lawsonite in CO<sub>2</sub>-bearing systems, isobaric *T*–*X*(CO<sub>2</sub>) projections have been calculated in the CaMASCH and CaFASCH model systems at 12, 14 and 16 kbar (Figs. 10 and S4). This *P* range covers the prograde to peak *P* conditions reached by the Combin Zone as constrained by the *P*–*T* modelling on the micaschist OL38 (Fig. 9). Additionally, the following reactions have also been plotted:



Whereas the topology of the invariant points and univariant curves is the same in the CaMASCH and CaFASCH systems, the equilibria are shifted towards higher *T* with increasing pressure (Figs. 10a, b and S4). The stability field of law + arag + q (blue field) expands with increasing *P* towards higher *T*, due to the displacement of the reaction



The reaction law = arag + ky + q restrains this field (and the stability of lawsonite in general) to *X*(CO<sub>2</sub>) < 0.022. For the calcschists, the maximum temperatures estimated by RSCM are in the range ~460–500 °C. This suggests that the presence of lawsonite, aragonite and quartz requires

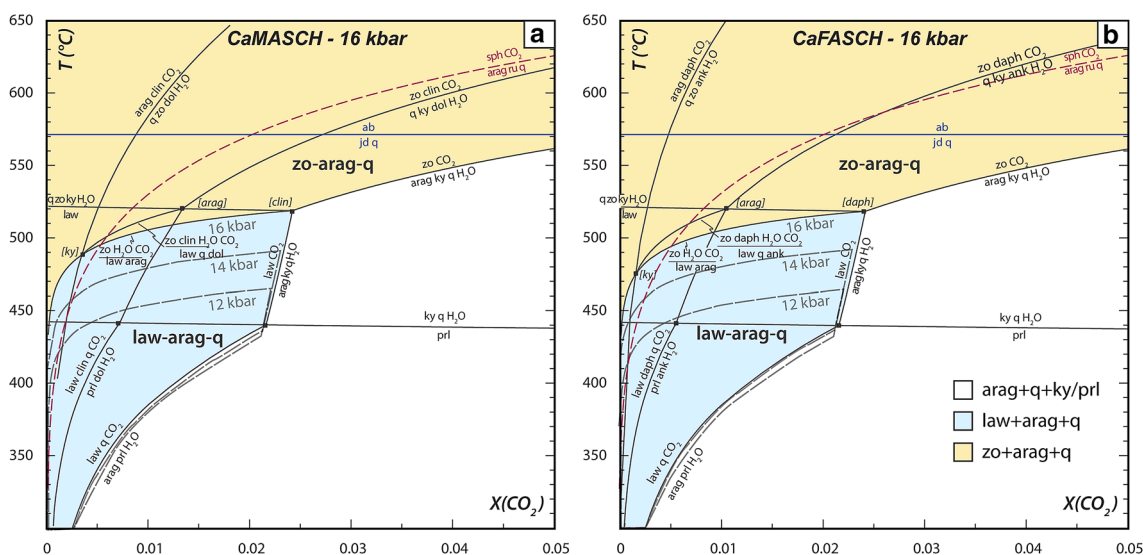


**Fig. 10** Isobaric *T*–*X*(CO<sub>2</sub>) projections/grids in the system CMASH and CFASH, calculated at a pressure of 16 kbar (**a**, **b**). The reaction albite = jadeite + quartz is plotted as a reference. The decarbonation equilibrium *ru* + arag + *q* = sph + CO<sub>2</sub> is also shown by a dashed red

line. The grey dashed lines show the effect of pressure on the reaction zo = law + arag. The blue and yellow fields indicate the *T*–*X*(CO<sub>2</sub>) space where lawsonite + aragonite + quartz and zoisite + aragonite + quartz, respectively, can be stable

fluids with very low  $X(\text{CO}_2)$  and a minimum  $P$  of the order of 12 kbar.

In addition, the coexistence of titanite with quartz and aragonite in the pseudomorphed lawsonite-bearing calcschist OL32, further constrains the  $X(\text{CO}_2)$  to extremely low values ( $<0.001$  at 12 kbar, and  $<0.006$  at 16 kbar, Fig. 10). Considering the measured composition of titanite and consequently its reduced activity ( $a_{\text{sph}} = 0.87$ ) has only a negligible effect on the position of equilibrium (2) ( $X(\text{CO}_2)$  increases by 0.001,  $T$  decreases by less than 5 °C).

## Discussion

### $P$ – $T$ history

On the basis of new field and petrological data two tectonic units may be identified within the Combin Zone. They differ in size, lithological content, and Alpine  $P$ – $T$  conditions. New petrological and field data also indicate that there is a major tectonic discontinuity between the two units constituting the Combin Zone west of the Dent Blanche nappe (Fig. 7). Each unit displays different, but homogeneous (within the error of the thermobarometric estimates) metamorphic peak  $P$ – $T$  conditions, with a  $T$  gap between the two units of ~50–80 °C.

### Cornet Unit

The upper unit, hereafter called the Cornet Unit, is structurally located just below the contact with the Dent Blanche nappe, and consists of 50–100-m-thick blackish phyllites and minor brownish calcschists. The last few metres below the contact with the overlying Dent Blanche nappe are made of a diverse array of ocean-derived lithologies, including serpentinite, and interpreted as a potential melange along the subduction interface (Angiboust et al. 2014; Manzotti and Ballèvre 2017). The Cornet Unit is discontinuously exposed along the western base of the Dent Blanche nappe. It crops out in the Col Cornet and Fenêtre de Durand areas (Figs. 2, 7). RSCM estimates (Fig. 7) show that the Cornet Unit experienced relatively low- $T$  conditions (370–400 °C) during the Alpine metamorphism (this study, Angiboust et al. 2014). The peak  $P$  conditions reached by this unit during the Alpine history are difficult to assess, due to the lack of diagnostic or  $P$ – $T$ -sensitive mineral assemblages. North of the studied area, RSCM  $T$  estimates may be used to define the same sub-unit within the Combin Zone, e.g. in the Aiguilles Rouges d’Arolla (Decrausaz et al. 2021) and Bréonaz (Negro et al. 2013; Angiboust et al. 2014).

### By Unit

The lower unit (hereafter referred to as the By Unit) is located on top of the Grand Saint Bernard nappe and underlies the Cornet Unit, or, if the latter is lacking, directly the Dent Blanche nappe. The By Unit contains by far most of the oceanic sediments and associated ophiolites within the Combin Zone (Figs. 2, 7), and it may prove upon further research to be a southern equivalent of the Tsaté nappe. The By Unit is dominated by carbonate rocks (i.e. calcschists interbedded with impure to pure marbles) with subordinate metabasalts and serpentinite slices, and minor meta-gabbros of N-MORB affinity (Manzotti et al. 2017). The metamorphic history of the By Unit is known through three types of data.

- Our RSCM estimates on the studied calcschists indicate a peak  $T$  in the range 450–500 °C for the Alpine metamorphism. These values are in good agreement with maximum  $T$  estimated by RSCM in the Combin Zone to the west of the Dent Blanche nappe (Negro et al. 2013; Angiboust et al. 2014).
- The prograde  $P$ – $T$  evolution of the studied garnet-bearing micaschist (sample OL38) during the Alpine cycle is marked by the growth of the garnet core at ~15 kbar, 410 °C (Fig. 9a) and the subsequent prograde evolution that peaked at 16–17 kbar and 460–480 °C (Fig. 9b). This stage represents the peak  $P$ – $T$  conditions reached by the By Unit during the Alpine cycle.
- Metamorphic aragonite inclusions in titanite and spectacular pseudomorphs after lawsonite in calcschists; these deserve a separate discussion.

The meta-sediments from the Saint Barthelemy valley (east of the Dent Blanche nappe) display characteristics similar to those of the By Unit, including the pseudomorphs after lawsonite.

### A first report of metamorphic aragonite inclusions in titanite

Metamorphic aragonite is seldom reported in blueschist-facies rocks, and this is generally ascribed to the fast kinetics of the polymorphic transition (Brown et al. 1962). Following experimental studies (Snow and Yund 1987; Hacker and Kirby 1993; Hacker et al. 2005) and theoretical considerations on the exact mechanism of the polymorphic transformation (Carlson and Rosenfeld 1981; Madon and Gillet 1984; Gillet et al. 1987; Sotin and Madon 1988), it is assumed that aragonite preservation is favoured if the transition is crossed along the exhumation path at a  $T$  lower than about 200–250 °C, in the absence of fluid and deformation. Such conditions have been rarely met in the Western Alps, and indeed the only occurrences so far reported is located in

the External Vanoise (Fig. 1), the coldest *HP* unit along this traverse (Gillet and Goffé 1988), and in the Lanzo Massif, where metamorphic aragonite is included in magnetite and garnet (Vitale Brovarone et al. 2017; Giuntoli et al. 2020).

No pseudomorphs after metamorphic aragonite (like those of Syros—Brady et al. 2004) have been found in the field, despite extensive research during mapping. This is attributable to the full aragonite recrystallisation (e.g. Seaton et al. 2009) during the pervasive greenschist-facies ductile deformation. Consequently, chances are weak to find relict aragonite in the matrix. On the other hand, aragonite could be preserved in a rheologically strong host mineral (Gillet et al. 1984; van der Molen and van Roermund 1986; Tajčmanová et al. 2021). Such a host happened to be titanite in our rocks. However, only very small crystals (5–10 µm), entirely included, distant from fractures, have yielded Raman spectra of aragonite, most other inclusions having been converted to calcite.

Interestingly, in the eclogite-facies rocks from the Piemonte-Liguria Ocean, metamorphic aragonite has been documented in Alpine Corsica (Chopin et al. 2008). There, rare marble samples display graphite-bearing parageneses with aragonite-grossular intergrowths. Such a growth mechanism is unrelated to the one observed in our samples, where aragonite is making globular inclusions inside its host, and there is no observation in support of a previous fibrous habit. Preservation of metamorphic aragonite in the Corsican samples has also been related to the mechanical behaviour of the host garnet. Although metamorphic aragonite inclusions in titanite are, to the best of our knowledge, reported here for the first time, aragonite inclusions have been already found in a large number of host species (garnet, e.g. Kouketsu and Enami 2010; omphacite, e.g. Proyer et al. 2013; diamond, e.g. Dobrzhinetskaya et al. 2006; zircon, e.g. Liu et al. 2001; allanite, e.g. Liu et al. 2015). We are quite confident that further examination of a larger amount of marbles or calc-schists from the Western Alps may reveal other metamorphic aragonite occurrences in titanite crystals.

### A first report of lawsonite in the Combin Zone

Many studies have been conducted in the Combin Zone in the last decades. Despite the report of the local occurrence garnet in manganese-rich meta-cherts (Burri et al. 1999) and of sodic amphibole in metabasites (i.e. magnesio-riebeckite: Angiboust et al. 2014), the recent detailed petrological and geochemical studies (Angiboust et al. 2014; Jaeckel et al. 2018; Epstein et al. 2020, 2021) have not reported lawsonite, and its lack along the section studied in this paper was even specifically emphasized. We are pleased now to have found this missing lawsonite. Indeed, this study presents the first description of pseudomorphs after lawsonite in the calc-schists of the Combin Zone (By Unit) and demonstrates that

lawsonite was stable during its prograde to peak *P–T* evolution (Fig. 10). Our thermodynamic modelling shows that at the peak *P–T* conditions derived from the RSCM data and the garnet micaschist, lawsonite–aragonite–quartz was the stable assemblage in the meta-marls, at the condition that  $X(\text{CO}_2)$  did not exceed 0.005 mol per cent in the titanite-bearing meta-marls. Further studies on the primary fluid inclusions (see e.g. Herviou et al. 2021) may provide additional constraints on the fluid composition in equilibrium with lawsonite.

### Lawsonite breakdown reactions

In a sense, lawsonite-breakdown reactions should be easy to investigate, because the products are under our eyes. However, great care should be taken in identifying breakdown products, because some of the phases actually occurring in the pseudomorphs may be former inclusions in the lawsonite porphyroblasts, known to contain a large amount of inclusions (e.g. Caron 1974; Lefeuvre et al. 2020). At least three phases can be safely considered as being co-stable with lawsonite rather than a breakdown product. The first two ones are titanite (e.g. sample OL32) and rutile (e.g. sample OL30), because of the immobility of titanium. The third one is graphite, especially when it defines curved lines interpreted as inclusion trails formed during synkinematic lawsonite growth (VB13, Fig. S3). In a single pseudomorph, one can note that graphite trails persist in albite, but are lacking in calcite, suggesting that carbon was consumed during the breakdown reaction, enhancing the growth of calcite.

Another point of concern is the fact that the material inside the pseudomorph is never isochemical with respect to lawsonite, and may vary considerably in adjacent lithologies (e.g. Felix and Fransolet 1972; Ballèvre et al. 2003; Hamelin et al. 2018). The presence of muscovite + paragonite (OL30) or muscovite + albite (OL32) within the pseudomorphs requires the addition of K and Na to the original lawsonite. In both samples, white micas in the pseudomorphs have a much lower celadonite content than those in the matrix, suggesting growth at lower *P–T* conditions.

The best example of a lawsonite-breakdown reaction was found in sample from the St Barthelemy valley (VB13, Fig. S3), where the pseudomorphs consist of zoisite and calcite and where zoisite is only found in the pseudomorphs, thus suggesting reaction (3) to have taken place.

### Timing of lawsonite growth and breakdown with respect to ductile deformation

Porphyroblasts in general (e.g. Zwart 1962; Passchier and Trouw 2005) and lawsonite in particular (e.g. Caron 1974) are useful markers for deciphering the timing of metamorphism with respect to deformation.

In sample OL30 (Fig. 5a, b), the unusually large pseudomorphs (with hourglass sector zoning) overgrow a faint layering ( $S_0$ ) which has been only weakly crenulated ( $S_1$ ). Most pseudomorphs are elongated at high angle with respect to  $S_0$ , and approximately parallel to  $S_1$ . This suggests that the main episode of growth has taken place before  $S_1$ .

In sample OL32, pseudomorphs after lawsonite locally, although rarely, preserve their original lozenge shape. In most cases, however, pseudomorphs after lawsonite are moderately deformed (Fig. 6a), which results in the formation of dissolution seams along some faces, and pressure shadows along the others. In the field, the orientation of these dissolution seams is parallel to the axial planes of  $F_2$  folds, and consequently probably related to stage 2 deformation. Lawsonite growth may have occurred in this sample either during or after the development of the  $S_1$  pervasive foliation.

In samples VB13 (Fig. S3) and VB21, lawsonite porphyroblasts overgrow a pervasive foliation nicely recorded by the alignment of tiny graphite crystals. Because this “internal foliation” ( $S_1$ ) is either straight or slightly curved, and is discontinuous with respect to the “external foliation” ( $S_2$ ), growth of lawsonite porphyroblasts has taken place during development of  $D_1$ .

Lawsonite breakdown has taken place during exhumation of the Combin Zone. Increasing strain associated with  $S_2$  may have led to a complete destruction of the pseudomorphs after lawsonite, that would become unrecognizable. This could explain why lawsonite was not recognized before this study. On the other hand, it may be used to map the domains, at regional scale, where intense greenschist-facies deformation has erased the pseudomorphed lawsonite, and therefore better define the strain gradients within the Combin Zone.

### Implications for the metamorphic structure of the Western Alps

These new data have important implications both for the metamorphic history of the oceanic units in the Western Alps and for the building of the nappe stack along the subduction interface.

#### Metamorphic structure of the Western Alps

After several decades of research, the metamorphic structure of the Western Alps is nicely depicted on the metamorphic maps of the Alps (e.g. Bousquet et al. 2012; Ballèvre et al. 2020). Concerning the oceanic units derived from the Piemonte–Liguria Ocean, Agard (2021) provides a synthesis where two types of units are distinguished (see introduction). The MUM-type units (Zermatt, Viso, Voltri), out of the scope of this paper, record an eclogite-facies metamorphism (Fig. 11). The S-type units, to which the Combin

Zone belongs, have been subdivided into low- $T$  blueschists (with preserved carpholite and lawsonite) and high- $T$  blueschists (where most carpholite is replaced by chloritoid and lawsonite by zoisite).

The section across the south-western Alps (Fig. 1) represents a reference section for the S-type units. There, a continuous gradient across the Queyras Unit has been evidenced. The western, lower  $T$  zone (Fraitève, Triplex in Fig. 11a) is characterized by abundant preserved lawsonite and carpholite (Agard et al. 2001; Lefeuvre et al., 2020), whereas the eastern, higher  $T$  zone (Assietta–Albergian in Fig. 11a) displays pseudomorphs after lawsonite (frequently containing zoisite) and chloritoid instead of carpholite (Agard et al. 2001). A ductile shear zone separates the Queyras blueschist-facies units from the Viso eclogite-facies units (i.e. Finestre, Monviso and Lago Superiore in Fig. 11a) (Ballèvre et al. 1990; Agard et al. 2001; Ghignone et al. 2020b).

Considering now the section in the north-western Alps (Fig. 1), many authors have proposed that the Combin Zone may represent an equivalent of the Queyras Unit, based on (i) the structural position of the Combin Zone, more internal than the Briançonnais Grand Saint Bernard nappes, and (ii) the lack of eclogite-facies parageneses, and the occurrence of rare relicts of blueschist-facies minerals (especially sodic amphiboles of magnesio-riebeckite to ferro-glaucophane compositions). However, neither lawsonite nor metamorphic aragonite were described in this area. Our findings, therefore, allow us to explain the paradox. The oldest metamorphic parageneses found in the largest part of the Combin Zone (By Unit in Fig. 11b) have crystallised in the lawsonite-aragonite stability field, at about 460–480 °C, 16–17 kbar. The uppermost part of the Combin Zone, occurring as smaller slices just below the overlying Dent Blanche nappe (Cornet Unit in Fig. 11b, but also Aiguilles Rouges d’Arolla Unit further north according to Decrausaz et al. 2021) is characterized by lower  $P$ – $T$  conditions than the By Unit. One major difference with respect to the south-western section of the Alps is that the most external domain, with fresh lawsonite and carpholite, is lacking in the north-western Alps, explaining why previous authors did not recognize the lawsonite-glaucophane zone or the lawsonite isograd in this transect.

#### $P$ – $T$ discontinuities in the nappe stack

In the north-western Alps, from the bottom to the top, the nappe stack involves the various units of the Grand Saint Bernard nappe (including their sedimentary cover), the oceanic rocks that constitute the bulk of the Combin Zone (Tsaté nappe, Aiguilles Rouges d’Arolla, By Unit...) and the overlying Dent Blanche nappe. The  $P$ – $T$  history of the Grand Saint Bernard subunits has not been the topic of recent research. Pending further studies (in course), the RSCM data

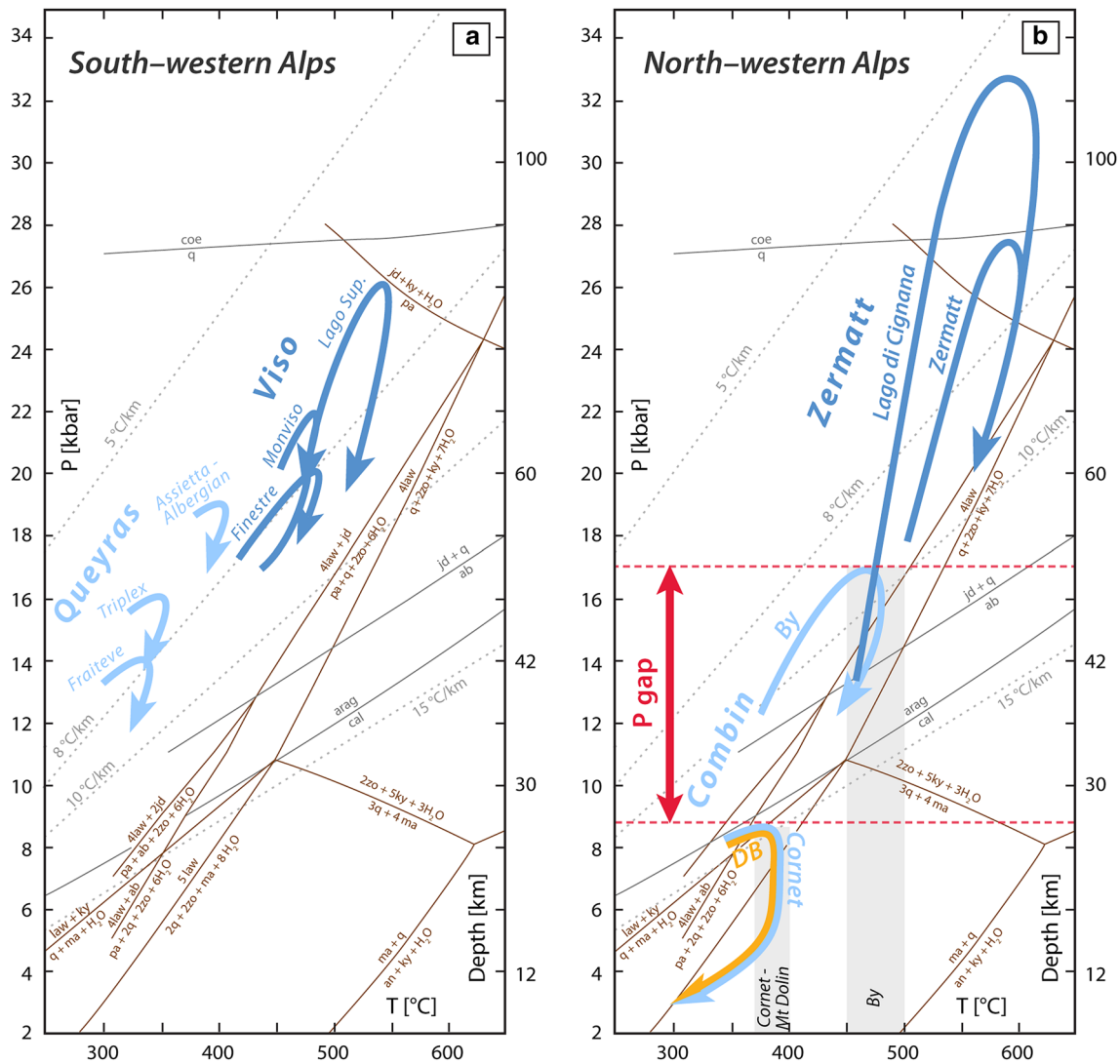


**Fig. 11** *P–T* diagrams showing the *P–T* paths followed by Piemonte-Liguria-derived units and Dent Blanche nappe (yellow trajectory in **b**) in the north-western and south-western Alps. The univariant reactions depicted in this figure have been calculated using THERMOCALC. *P–T* paths from blueschist-facies and eclogite-facies units are depicted in light and dark blue, respectively. The two grey bands in (**b**) represent the estimated RSCM ranges of maximum *T* for the Cornet and By units, respectively. **a** South-western Alps: *P–T* paths are

taken from the literature for the Queyras (Fraiteve, Triplex, Assietta-Albergian: Agard et al. 2001) and Viso units (Finestre: Agard et al. 2001; Lago Superiore: Groppo and Castelli 2010). **b** North-western Alps: metamorphic conditions are derived from this study for the By and Cornet Units; and from the literature for the other units (Dent Blanche nappe (DB): Manzotti et al. 2020; Zermatt Zone and Lago di Cignana Unit: Groppo et al. 2009)

for the Mesozoic cover of the higher subunit of the Grand Saint Bernard nappe (i.e. the Mont Fort nappe: see Pantet et al. 2020 for a discussion) have given values of the order of 450–500 °C (Fig. 7), similar to those in the overlying units. Further work is required to integrate in this scheme the “Série Rousse”, which is considered in our scheme (Fig. 7) as part of the detached cover from the Middle Penninic Units (see also Pantet et al. 2020).

In the oceanic units of the Western Alps, the thermobaric structure may be described using three end-member models, namely (i) a continuous *T* gradient across the oceanic

units, without *P* gaps, (ii) a continuous *T* gradient with *P* gaps, and (iii) distinct subunits with gaps in both *P* and *T* (e.g. Ballèvre et al. 1990; Agard et al. 2001; Plunder et al. 2012). Concerning specifically the case of the oceanic units of the Combin zone, Angiboust et al. (2014) have suggested the occurrence of three subunits displaying a continuous *T* gradient, i.e. from the bottom to the top a lower subunit with a max. *T* in the range 490–460 °C, a median subunit with a max. *T* in the range 450–420 °C, and an upper subunit with a max. *T* in the range 410–360 °C. However, it is unclear in the model of Angiboust et al. (2014) whether the subunits

are separated by gaps either in  $P$ ,  $T$ , or both and their (tectonic?) boundaries have not been drawn on a map. Given the large and consistent dataset now available on maximum  $T$  derived from RSCM data (Negro et al. 2013; Angiboust et al. 2014; Decrausaz et al. 2021; this paper), we recognize in the studied area the existence of two main units (Cornet and By units) with a  $T$  gap of the order of at least 50 °C. In agreement with this  $T$  difference, and independently of the estimation method, we found garnet and lawsonite only in the higher  $T$ , structurally lower, unit (i.e. By unit). The lower  $T$ , structurally higher, unit (i.e. Cornet Unit) may be extended further north, out of the studied area, and includes slices located below the basal contact of the Dent Blanche nappe stack, the largest slice being the Aiguilles Rouges d'Arolla (Decrausaz et al. 2021). Given the  $T$  gap between them, we consider that the By and Cornet units are separated by a tectonic boundary (Fig. 7).

In the Dent Blanche nappe,  $P$ – $T$  conditions of  $8 \pm 1$  kbar ~ 400 °C have been recently estimated by thermodynamic modelling in rocks cropping out in the Ollomont valley close to the contact with the Cornet Unit (Manzotti et al. 2020). These values are consistent with the relatively low  $T$  conditions ( $387 \pm 14$  °C; Angiboust et al. 2014) previously estimated for the Mont Dolin Series (i.e. the Mesozoic cover) of the Dent Blanche nappe exposed farther north, close to the Arolla village (Fig. 7). On the basis of these data, it may be suggested that the Dent Blanche nappe and the Cornet Unit may have reached similar peak  $P$ – $T$  conditions ( $8 \pm 1$  kbar and ~ 400 °C) conditions during the Alpine cycle (Fig. 11b). If so, the Cornet and By Units record a  $P$  difference of ~ 8 kbar (~ 20–25 km) during the Alpine metamorphism (Fig. 11b) and their interface represents a major tectonic contact.

The timing of the peak  $P$ – $T$  conditions remains a matter of debate and is still poorly constrained (see Manzotti et al. 2014a for a detailed discussion). In the Dent Blanche nappe, K–Ar ages scatter from 55 to 30 Ma (Mont Dolin: Ayrton et al. 1982), whereas Rb–Sr ages display a range from 58 to 43 Ma (Angiboust et al. 2014), interpreted as recording a protracted evolution of the deformation under high-pressure metamorphic conditions. In the Combin Zone, Rb–Sr geochronology on white mica constrains the greenschist-facies deformation at 45–36 Ma (Reddy et al. 1999, Reddy et al. 2003; Angiboust et al. 2014).

To sum up, there is a significant metamorphic discontinuity between the bulk of the ocean-derived units from the Combin Zone and the overlying Dent Blanche nappe. This contact, whose detailed description is out of scope of this paper, has been interpreted as a ductile normal shear zone post-dating the early, subduction-related, fabrics (Ballèvre and Manzotti 2020).

## Conclusions

The main conclusions of this study are as follows.

1. We discovered lawsonite and metamorphic aragonite in the Combin Zone, confirming the supposed but poorly documented blueschist-facies character of the Combin Zone. It is only the third finding of metamorphic aragonite in the Western Alps.
2. Lawsonite can be stable in impure metacarbonates, but only at very low  $X(\text{CO}_2)$ . Its presence implies  $P > 12$  kbar for the temperatures estimated by RSCM (450–500 °C).
3. Thermodynamic modelling shows peak  $P$ – $T$  conditions of 16–17 kbar at 460–480 °C for the largest part of the Combin Zone (By Unit). These pressures are ~ 8 kbar higher than those of the overlying Dent Blanche, indicating the presence of a major tectonic contact, interpreted as a ductile normal shear zone. This contact cuts across the meta-sedimentary series and divides the Combin zone into the By and Cornet units.

**Supplementary Information** The online version contains supplementary material available at <https://doi.org/10.1007/s00410-021-01818-0>.

**Acknowledgements** This study was inspired by questions from Christophe Real who pointed ‘strange’ mica aggregates in calcschists, similar to those in the Cignana area he was mapping during his Master work. Jessica Langlade (Microsonde Ouest, Brest, France) and Martin Robyr (University of Lausanne, Switzerland) are thanked for assistance during EPMA data acquisition. Paola Manzotti was financially supported by the Swiss National Science Foundation (Ambizione project PZ00P2\_161202) and by a Starting Grant (Fund 4615701) of Stockholm University. Michel Ballèvre acknowledges no funding for travel expenses and field work. Christian Chopin and an anonymous reviewer are thanked for their constructive reviews. The editorial work of Hans Keppler has been highly appreciated.

**Funding** Open access funding provided by Stockholm University.

**Open Access** This article is licensed under a Creative Commons Attribution 4.0 International License, which permits use, sharing, adaptation, distribution and reproduction in any medium or format, as long as you give appropriate credit to the original author(s) and the source, provide a link to the Creative Commons licence, and indicate if changes were made. The images or other third party material in this article are included in the article’s Creative Commons licence, unless indicated otherwise in a credit line to the material. If material is not included in the article’s Creative Commons licence and your intended use is not permitted by statutory regulation or exceeds the permitted use, you will need to obtain permission directly from the copyright holder. To view a copy of this licence, visit <http://creativecommons.org/licenses/by/4.0/>.

## References

- Agard P (1999) Evolution métamorphique et structurale des métapélites océaniques dans l'orogène alpin: l'exemple des schistes lustrés des Alpes occidentales (Alpes Cottiennes). PhD Dissertation. Université Pierre et Marie Curie, Paris VI, 184 pp
- Agard P (2021) Subduction of oceanic lithosphere in the Alps: selective archetypal from (slow-spreading) ocean. *Earth Sci Rev* 214:103517
- Agard P, Lemoine M (2005) Faces of the Alps. Structure and geodynamic evolution. Commission for the geological map of the world, 48 pp
- Agard P, Jolivet L, Goffé B (2001) Tectonometamorphic evolution of the Schistes Lustrés complex: implications for the exhumation of HP and UHP rocks in the Western Alps. *Bull Soc Geol Fr* 172:17–636
- Angiboust S, Glodny J (2020) Exhumation of eclogitic ophiolitic nappes in the W. Alps: new age data and implications for crustal wedge dynamics. *Lithos* 356–357:105374
- Angiboust S, Agard P, Jolivet L, Beyssac O (2009) The Zermatt-Saas ophiolite: the largest (60–km wide) and deepest (c. 70–80 km) continuous slice of oceanic lithosphere detached from a subduction zone. *Terra Nova* 21:171–180
- Angiboust S, Langdon R, Agard P, Waters D, Chopin C (2012) Eclogitization of the Monviso ophiolite (W. Alps) and implications on subduction dynamics. *J Metamorph Geol* 30:37–61
- Angiboust S, Glodny J, Oncken O, Chopin C (2014) In search of transient subduction interfaces in the Western Alps subduction system. *Lithos* 205:298–321
- Ayrton S, Bugnon C, Haarpainter T, Weidmann M, Frank E (1982) Géologie du front de la nappe de la Dent Blanche dans la région des Monts-Dolins, Valais. *Eclogae Geol Helv* 75:269–286
- Baldelli C, Dal Piaz GV, Polino R (1983) Le quarziti a manganese e cromo di Varenche–St. Barthélémy, una sequenza di copertura oceanica della falda piemontese. *Ofoliti* 8:207–221
- Ballèvre M, Lagabrielle Y (1994) Garnet in blueschist facies marbles from the Queyras unit (Western Alps): its occurrence and its significance. *Schweiz Miner Petrogr Mitt* 74:203–212
- Ballèvre M, Lagabrielle Y, Merle O (1990) Tertiary ductile normal faulting as a consequence of lithospheric stacking in the Western Alps. *Mém Soc Géol Fr* 156:227–236
- Ballèvre M, Manzotti P (2020) Exhumation of HP/UHP rocks by normal ductile shearing on top of the Eocene extruding wedge. *EGU2020-10771*. <https://doi.org/10.5194/egusphere-egu2020-18271>
- Ballèvre M, Pitra P, Bohn M (2003) Lawsonite growth in the epidote blueschists from Ile de Groix (Armorican Massif, France): a potential geobarometer. *J Metamorph Geol* 21:723–735
- Ballèvre M, Camonin A, Manzotti P, Poujol M (2020) A step towards unravelling the paleogeographic attribution of pre-Mesozoic basement complexes in the Western Alps based on U-Pb geochronology of Permian magmatism. *Swiss J Geosci* 113:12. <https://doi.org/10.1186/s00015-020-00367-1>
- Bearth P (1962) Versuch einer Gliederung alpinmetamorpher Serien der Westalpen. *Schweiz Miner Petrogr Mitt* 42:127–137
- Bearth P (1966) Zur mineralfaziellen Stellung der Glaukophan-Gesteine der Westalpen. *Schweiz Miner Petrogr Mitt* 46:13–23
- Bearth P (1967) Die Ophiolite der Zone von Zermatt-Saas Fee. *Beitr Geol Karte Schweiz* 132:1–130
- Bearth P (1973) Gesteins- und Mineralparagenesen aus den Ophiolithen von Zermatt. *Schweiz Miner Petrogr Mitt* 44:15–26
- Bebout GE, Agard P, Kobayashi K, Moriguti T, Nakamura E (2013) Devolatilization history and trace element mobility in deeply subducted sedimentary rocks: evidence from Western Alps HP/UHP suites. *Chem Geol* 342:1–20
- Beyssac O, Goffé B, Chopin C, Rouzaud JN (2002) Raman spectra of carbonaceous material in metasediments: a new geothermometer. *J Metamorph Geol* 20:859–871
- Beyssac O, Goffé B, Petitot JP, Froigneux E, Moreau M, Rouzaud JN (2003) On the characterization of disordered and heterogeneous carbonaceous materials using Raman spectroscopy. *Spectrochim Acta A* 59:2267–2276
- Bigi G, Cosentino D, Coli M, Parotto M, Sartori R, Scandone P (1983) Structural model of Italy, sheet no. 1, 1: 500,000. CNR, Italy
- Bocquet J (1971) Cartes de répartition de quelques minéraux du métamorphisme alpin dans les Alpes franco-italiennes. *Eclogae Geol Helv* 64:71–103
- Bocquet J (1974) Études minéralogiques et pétrologiques sur les métamorphismes d'âge alpin dans les Alpes françaises. Habilitation Thesis, Univ Grenoble, 489 pp
- Bousquet R, Engi M, Gosso G, Oberhänsli R, Berger A, Spalla MI, Zucali M, Goffé B (2004) Explanatory notes to the map: metamorphic structure of the Alps—transition from the Western to the Central Alps. *Mitt Österr Miner Ges* 149:145–156
- Bousquet R, Oberhänsli R, Goffé B, Wiederkehr M, Koller F, Schmid SM, Schuster R, Engi M, Berger A, Martinotti M (2008) Metamorphism of metasediments at the scale of an orogeny: a key to Tertiary geodynamic of the Alps. In: Siegesmund S, Fügenschuh B, Froitzheim N (eds) *Tectonic aspects of the Alpine–Dinaride–Carpathian System*, vol 298. *Geol Soc London Spec Publ*, London, pp 393–411
- Bousquet R, Oberhänsli R, Schmid SM, Berger A, Wiederkehr M, Robert C, Möller A, Rosenberg C, Zeilinger G, Molli G, Koller F (2012) Metamorphic framework of the Alps. Commission for the geological map of the world; subcommission for magmatic and metamorphic maps. IUGS and IUGG, Paris. Retrieved from <http://www.ccgmg.org>
- Brady JB, Markley MJ, Schumacher JC, Cheney JT, Banciardi GA (2004) Aragonite pseudomorphs in high-pressure marbles of Syros, Greece. *J Struct Geol* 26:3–9
- Brown WH, Fyfe WS, Turner FJ (1962) Aragonite in California glaucophane schists, and the kinetics of the aragonite-calcite transition. *J Petrol* 3:566–587
- Bucher K, Grapes R (2009) The eclogite-facies Allalin gabbro of the Zermatt-Saas ophiolite, Western Alps: a record of subduction zone hydration. *J Pet* 50:1405–1442
- Burri M, Dal Piaz GV, Della Valle G, Gouffon Y, Guermani A (1999) Notice explicative, feuille 1346 Chanrion, avec partie nord de la feuille 1366 Mont Vélan. *Atlas Géologique de la Suisse* 1:25000, vol 101, pp 4–79
- Carignan J, Hild P, Mevelle G, Morel J, Yeghicheyan D (2001) Routine analyses of trace elements in geological samples using flow injection and low pressure on-line liquid chromatography coupled to ICP-MS: a study of geochemical reference materials, BR, DRN, UB-N, AN-G and GH. *Geostandard Newslett* 25:187–198
- Carlson WD, Rosenfeld JL (1981) Optical determination of topotactic aragonite-calcite growth kinetics—metamorphic implications. *J Geol* 89:615–638
- Caron JM (1974) Rapports entre diverses “générations” de lawsonite et les déformations dans les Schistes lustrés des Alpes cottiennes septentrionales (France et Italie). *Bull Soc Géol Fr* S7-XVI (3):255–263
- Chopin C, Beyssac O, Bernard S, Malavieille J (2008) Aragonite-garnet intergrowths in eclogite-facies marble, Alpine Corsica. *Eur J Miner* 20:857–865
- Clarke GL, Powell R, Fitzherbert JA (2006) The lawsonite paradox: a comparison of field evidence and mineral equilibria modelling. *J Metamorph Geol* 24:715–725
- Coggon R, Holland TJB (2002) Mixing properties of phengitic micas and revised garnet–phengite thermobarometers. *J Metamorph Geol* 20:683–696

- Cogulu E (1967) Etude pétrographique de la région de Mihaliccik (Turquie). *Schweiz Miner Petrogr Mitt* 47:683–824
- Coleman RG, Lee DE (1962) Metamorphic aragonite in the glaucophane schists of Cazadero, California. *Am J Sci* 260:577–595
- Compagnoni R (1977) The Sesia-Lanzo Zone: high pressure-low temperature metamorphism in the Austroalpine continental margin. *Rend Soc Ital Min Petrol* 33:335–378
- Dal Piaz GV (1974) Le métamorphisme de haute pression et basse température dans l'évolution structurale du bassin ophiolitique alpino-apyenninique (2e partie). *Schweiz Miner Petrogr Mitt* 54:399–424
- Dal Piaz GV, Bistacchi A, Gianotti F, Monopoli B, Passeri L (2015) Note illustrative della carta Geologica d'Italia alla scala 1:50000. Foglio 070, Cervino. Servizio Geologico d'Italia, Roma, pp 1–431
- de Capitani C, Brown TH (1987) The computation of chemical equilibrium in complex systems containing non-ideal solutions. *Geochim Cosmochim Acta* 51:2639–2652
- de Capitani C, Petrakakis K (2010) The computation of equilibrium assemblage diagrams with Theriak/Domino software. *Am Miner* 95:1006–1016
- Decrausaz T, Müntener O, Manzotti P, Lafay R, Spandler C (2021) Fossil oceanic core complexes in the Alps. New field, geochemical and isotopic constraints from the Tethyan Aiguilles Rouges Ophiolite (Val d'Hérens, Western Alps, Switzerland). *Swiss J Geosci* 114:3. <https://doi.org/10.1186/s00015-020-00380-4>
- De Wever P, Caby R (1981) Datation de la base des schistes lustrés postophiolitiques par des radiolaires (Oxfordien supérieur-Kimmeridgien moyen) dans les Alpes Cottiniennes (Saint-Véran, France). *C R Acad Sci Paris* 292:467–472
- Diener JFA, Powell R (2012) Revised activity-composition models for clinopyroxene and amphibole. *J Metamorph Geol* 30:131–142
- Dobrzynetskaia LF, Wirth R, Green HW II (2006) Nanometric inclusions of carbonates in Kokchetav diamonds from Kazakhstan: a new constraint for the depth of metamorphic diamond crystallization. *Earth Planet Sci Lett* 343:85–93
- Dragovic B, Angiboust S, Tappa MJ (2020) Petrochronological close-up on the thermal structure of a paleo-subduction zone (W. Alps). *Earth Planet Sci* 547:116446
- Ellenberger F (1960) Sur une paragenèse éphémère à lawsonite et glaucophane dans le métamorphisme alpin en Haute-Maurienne (Savoie). *Bull Soc Géol Fr* S7-II (2):190–194
- Epstein GS, Bebout GE, Angiboust S, Agard P (2020) Scale of fluid-rock interaction and carbon mobility in the deeply underplated and HP-metamorphosed Schistes Lustrés, Western Alps. *Lithos* 354–355:105229
- Epstein GS, Bebout GE, Angiboust S (2021) Fluid and mass transfer along transient subduction interfaces in a deep paleo-accretionary wedge (Western Alps). *Chem Geol* 559:119920
- Ernst WG (1965) Mineral parageneses in Franciscan metamorphic rocks, Panoche Pass, California. *Geol Soc Am Bull* 76:879–914
- Ernst WG, Dal Piaz GV (1978) Mineral parageneses of eclogitic rocks and related mafic schists of Piemonte ophiolite nappe, Breuil-St-Jacques Area, Italian Western Alps. *Am Miner* 63:621–640
- Evans BW, Misch P (1976) A quartz-aragonite-talc schist from the lower Skagit Valley, Washington. *Am Miner* 61:1005–1008
- Felix C, Fransolet AM (1972) Pseudomorphes à épidote s.l., aragonite, muscovite s.l., chlorite, albite, ... de porphyroblastes de lawsonite (?) dans les glaucophanites de l'île de Groix (Bretagne – France). *Ann Soc Géol Belg* 95:323–334
- Fornash KF, Whitney DL, Seaton NCA (2019) Lawsonite composition and zoning as an archive of metamorphic processes in subduction zones. *Geosphere* 15:24–46
- Fry N, Fyfe WS (1971) On the significance of the eclogite facies in Alpine metamorphism. *Verh Geol B* 2:257–265
- Gabalda S, Beyssac O, Jolivet L, Agard P, Chopin C (2009) Thermal structure of a fossil subduction wedge in the Western Alps. *Terra Nova* 21:28–34
- Garofalo PS (2012) The composition of Alpine marine sediments (Bündnerschieder Formation, W Alps) and the mobility of their chemical components during orogenic metamorphism. *Lithos* 128–131:55–72
- Ghignone S, Borghi A, Balestro G, Castelli D, Gattiglio M, Groppo C (2020a) HP-tectonometamorphic evolution of the Internal Piedmont Zone in Susa Valley (Western Alps): new petrologic insight from garnet+chloritoid-bearing micaschists and Fe-Ti metagabbro. *J Metamorph Geol*. <https://doi.org/10.1111/jmg.12574>
- Ghignone S, Balestro G, Gattiglio M, Borghi A (2020b) Structural evolution along the Susa Shear Zone: the role of a first-order shear zone in the exhumation of meta-ophiolite units (Western Alps). *Swiss J Geosci* 113:17
- Gillet P, Goffé B (1988) On the significance of aragonite occurrences in the Western Alps. *Contrib Miner Petrol* 99:70–81
- Gillet P, Gérard Y, Willaime C (1987) The calcite–aragonite transition: mechanism and microstructures induced by the transformation stresses and strain. *Bull Minér* 110:481–496
- Gillet P, Ingrin J, Chopin C (1984) Coesite in subducted continental crust: P-T history deduced from an elastic model. *Earth Planet Sci Lett* 70:426–436
- Giuntoli F, Vitale Brovarone A, Menegon L (2020) Feedback between high-pressure genesis of abiogenic methane and strain localization in subducted carbonate rocks. *Sci Rep* 10:9848
- Goffé B, Chopin C (1986) High-pressure metamorphism in the Western Alps: zoneography of metapelites, chronology and consequences. *Schweiz Miner Petrogr Mitt* 66:41–52
- Goffé B, Schwartz S, Lardeaux JM, Bousquet R (2004) Explanatory notes to the map: metamorphic structure of the Alps – Western and Ligurian Alps. *Mitt Österr Miner Ges* 149:125–144
- Groppo C, Castelli D (2010) Prograde P-T evolution of a lawsonite eclogite from the Monviso meta-ophiolite (Western Alps): dehydration and redox reactions during subduction of oceanic FeTi-oxide gabbro. *J Petrol* 51:2489–2514
- Groppo C, Beltrando M, Compagnoni R (2009) The P-T path of the ultra-high pressure Lago di Cignana and adjoining high pressure meta-ophiolitic units: Insights into the evolution of the subducting Tethyan slab. *J Metamorph Geol* 27:207–231
- Guitard G, Saliot P (1970) Rôle des constituants fluides sur la stabilité et la nature des associations à lawsonite et à pumpellyite de certaines roches basiques et intermédiaires des Alpes de Savoie. *C R Acad Sci Paris* 271:8–15
- Hacker BR, Kirby SH (1993) High-pressure deformation of calcite marble and its transformation to aragonite under non-hydrostatic conditions. *J Struct Geol* 15:1207–1222
- Hacker BR, Rubie DC, Kirby SH, Bohlen SR (2005) The calcite–aragonite transformation in low-Mg marble: equilibrium relations, transformation mechanisms, and rates. *J Geophys Res Solid Earth* B03205
- Hamelin C, Brady JB, Cheney JT, Schumacher JC, Able LM, Sperry AJ (2018) Pseudomorphs after lawsonite from Syros, Greece. *J Petrol* 59:2353–2384
- Hawkins AT, Selverstone J, Brearley AJ, Beane RJ, Ketchum RA, Carlson WD (2007) Origin and mechanical significance of honeycomb garnet in high-pressure metasedimentary rocks from the Tauern window, Eastern Alps. *J Metamorphic Geol* 25:565–583
- Henry C, Burkhard M, Goffé B (1996) Evolution of synmetamorphic veins and their wallrocks through a Western Alps transect: no evidence for large-scale fluid flow. Stable isotope, major- and trace-element systematics. *Chem Geol* 127:81–109
- Hervieu C, Verlaquet A, Agard P, Locatelli M, Raimbourg H, Lefeuvre B, Dubacq B (2021) Along-dip variations of subduction fluids:

- The 30–80 km depth traverse of the Schistes Lustrés complex (Queyras-Monviso, W. Alps). *Lithos* 394–395:106168
- Holland TJB, Powell R (1998) An internally consistent thermodynamic data set for phases of petrological interest. *J Metamorph Geol* 16:309–343
- Holland TJB, Powell R (2003) Activity–composition relations for phases in petrological calculations: an asymmetric multicomponent formulation. *Contrib Miner Petrol* 145:492–501
- Holland TJB, Baker J, Powell R (1998) Mixing properties and activity composition and relationships of chlorites in the system MgO–FeO–Al<sub>2</sub>O<sub>3</sub>–SiO<sub>2</sub>–H<sub>2</sub>O. *Eur J Miner* 10:395–406
- Houfflain B, Caby R (1987) Rétrocharrriages précoces en climat schiste bleu à lawsonite-grenat: la “bande d’Acceglio-Longet” (Alpes Cottiennes). *C R Acad Sci Paris* 304:199–204
- Jaekel K, Bebout G, Angiboust S (2018) Deformation-enhanced fluid and mass transfer along Western and Central Alps paleo-subduction interfaces: significance for carbon cycling models. *Geosphere* 14:6. <https://doi.org/10.1130/GES01587.1>
- Johannes W, Puhani D (1971) The calcite-aragonite transition, reinvestigated. *Contrib Miner Petrol* 31:28–38
- Kaczmarek MA, Müntener O, Rubatto D (2008) Trace element chemistry and U–Pb dating of zircons oceanic gabbros and their relationship with whole rock composition (Lanzo, Italian Alps). *Contrib Miner Petrol* 155:295–312
- Kempf ED, Hermann J, Reusser E, Baumgartner LP, Lanari P (2020) The role of the antigorite + brucite to olivine reaction in subducted serpentinites (Zermatt, Switzerland). *Swiss J Geosci* 113:16. <https://doi.org/10.1186/s00015-020-00368-0>
- Kienast JR (1973) Sur l’existence de deux séries différentes au sein de l’ensemble “Schistes lustrés-ophiolites” du Val d’Aoste; quelques arguments fondés sur l’étude des roches métamorphiques. *CR Acad Sci Paris D276:2621–2624*
- Kienast JR, Velde B (1970) Le métamorphisme alpin dans les Alpes franco-italiennes: mise en évidence d’un gradient de température et de pression. *CR Acad Sci Paris D271:637–640*
- Kouketsu Y, Enami M (2010) Aragonite and omphacite-bearing metapelite from Besshi region, Sambagawa belt in central Shikoku, Japan and its implication. *Island Arc* 19:165–176
- Le Bayon B, Pitra P, Ballèvre M, Bohn M (2006) Reconstructing P–T paths during continental collision using multi-stage garnet (Gran Paradiso nappe, Western Alps). *J Metamorph Geol* 24:477–496
- Le Breton E, Brune S, Ustaszewski K, Zahirovic S, Seton M, Müller RD (2021) Kinematics and extent of the Piemont-Liguria Basin—implications for subduction processes in the Alps. *Solid Earth*. <https://doi.org/10.5194/se-2020-161>
- Lefevre B, Agard P, Verlaquet A, Dubacq B, Plunder A (2020) Massive formation of lawsonite in subducted sediments from the Schistes Lustrés (W. Alps): implications for mass transfer and decarbonation in cold subduction zones. *Lithos* 370–371:105629
- Liu J, Ye K, Maruyama S, Cong B, Fan H (2001) Mineral inclusions in zircon from gneisses in the ultrahigh-pressure zone of the Dabie Mountains, Asia. *J Geol* 109:523–535
- Liu P, Wu Y, Chen Y, Zhang J, Jin Z (2015) UHP impure marbles from the Dabie Mountains: metamorphic evolution and carbon cycling in continental subduction zones. *Lithos* 212–215:280–297
- Lombardo B, Rubatto D, Castelli D (2002) Ion microprobe U–Pb dating of zircon from a Monviso metaplagiograne: implications for the evolution of the Piedmont-Liguria Tethys in the Western Alps. *Ophioliti* 27:109–117
- López-Carmona A, Abati J, Pitra P, Lee JKW (2014) Retrogressed lawsonite blueschist from the NW Iberian Massif: P–T constraints from thermodynamic modelling and <sup>40</sup>Ar/<sup>39</sup>Ar geochronology. *Contrib Miner Petrol* 167:987
- Madon M, Gillet P (1984) A theoretical approach to the kinetics of calcite=aragonite transition: application to laboratory experiments. *Earth Planet Sci Lett* 67:400–414
- Mahar EM, Baker J, Powell R, Holland TJB, Howell N (1997) The effect of Mn on mineral stability in metapelites. *J Metamorph Geol* 15:223–238
- Manzotti P, Ballèvre M (2017) Tectonic history of the Dent Blanche. *Geol Field Trips* 9:1–73
- Manzotti P, Ballèvre M, Zucali M, Robyr M, Engi M (2014a) The tectonometamorphic evolution of the Sesia-Dent Blanche nappes (internal Western Alps): review and synthesis. *Swiss J Geosci* 107:309–336
- Manzotti P, Zucali M, Robyr M, Engi M (2014b) Geometry and kinematics of the Roisan-Cignana Shear Zone, and the orogenic evolution of the Dent Blanche Tectonic System. *Swiss J Geosci* 107:23–47
- Manzotti P, Ballèvre M, Dal Piaz GV (2017) Continental gabbros in the Dent Blanche Tectonic System (Western Alps): from the pre-Alpine crustal structure of the Adriatic palaeomargin to the geometry of an alleged subduction interface. *J Geol Soc Lond* 174:541–556
- Manzotti P, Ballèvre M, Pitra P, Putlitz B, Robyr M, Müntener O (2020) The growth of sodic amphibole at the greenschist- to blueschist-facies transition (Dent Blanche, Western Alps): bulk-rock chemical control and thermodynamic modelling. *J Petrol* 61:egaa044. <https://doi.org/10.1093/petrology/egaa044>
- Marthaler M, Stampfli GM (1989) Les Schistes lustrés à ophiolites de la nappe du Tsaté: un ancien prisme d’accrétion issu de la marge active apulienne? *Schweiz Miner Petrogr Mitt* 69:211–216
- Martin S, Cortiana G (2001) Influence of the whole-rock composition on the crystallization of sodic amphiboles (Piemonte Zone, Western Alps). *Ophioliti* 26:445–456
- Martin LAJ, Rubatto D, Vitale Brovarone A, Hermann J (2011) Late Eocene lawsonite-eclogite metasomatism of a granulite sliver associated to ophiolites in Alpine Corsica. *Lithos* 125:620–640
- McCarthy A, Tugend J, Mohn G, Candiotti L, Chelle-Michou C, Arculus R, Schmalholz SM, Müntener O (2020) A case of Ampferer-type subduction and consequences for the Alps and Pyrenees. *Am J Sci* 320:313–372
- McKee B (1962) Aragonite in the Franciscan rocks of the Pacheco Pass area, California. *Am Miner* 47:379–387
- Michard A (1967) Etudes géologiques dans les zones internes des Alpes cottiennes. CNRS éditions, Paris, p 447. Retrieved from <https://tel.archives-ouvertes.fr/tel-00802836>
- Michard A, Avigad D, Goffé B, Chopin C (2004) The high-pressure metamorphic front of the south Western Alps (Ubaye–Maira transect, France, Italy). *Schweiz Miner Petrogr Mitt* 84:215–235
- Mulcahy SR, King RL, Vervoort JD (2009) Lawsonite Lu–Hf geochronology: a new geochronometer for subduction zone processes. *Geology* 37:987–990
- Negro F, Bousquet R, Vils F, Pellet CM, Hänggi-Schaub J (2013) Thermal structure and metamorphic evolution of the Piemont-Liguria metasediments in the northern Western Alps. *Swiss J Geosci* 106:63–78
- Newton RC, Kennedy GC (1963) Some equilibrium reactions in the join CaAl<sub>2</sub>Si<sub>2</sub>O<sub>8</sub>–H<sub>2</sub>O. *J Geophys Res* 68:2967–2983
- Nitsch KH (1972) Das P–T–XCO<sub>2</sub>–Stabilitätsfeld von Lawsonit. *Contrib Miner Petrol* 34:116–134
- Okamoto A, Shimizu H, Fukuda JI, Muto J, Okudaira T (2017) Reaction-induced grain boundary cracking and anisotropic fluid flow during prograde devolatilization reactions within subduction zones. *Contrib Miner Petrol* 172:75
- Okay AI (1982) Incipient blueschist metamorphism and metasomatism in the Tavsanli region, Northwest Turkey. *Contrib Miner Petrol* 79:361–367
- Pantet A, Epard JL, Masson H (2020) Mimicking Alpine thrusts by passive deformation of synsedimentary normal faults: a record of the Jurassic extension of the European margin (Mont Fort nappe,

- Pennine Alps). *Swiss J Geosci* 113:13. <https://doi.org/10.1186/s00015-020-00366-2>
- Passchier CW, Trouw RAJ (2005) *Microtectonics*. Springer Verlag, Berlin-Heidelberg, p 366
- Philippon M, Gueydan F, Pitra P, Brun JP (2013) Preservation of subduction-related prograde deformation in lawsonite pseudomorph-bearing rocks. *J Metamorph Geol* 31:571–583
- Plunder A, Agard P, Dubacq B, Chopin C, Bellanger M (2012) How continuous and precise is the record of P-T paths? Insights from combined thermobarometry and thermodynamic modelling into subduction dynamics (Schistes Lustrés, W. Alps). *J Metamorph Geol* 30:323–346
- Pognante U (1989) Lawsonite, blueschist and eclogite formation in the southern Sesia zone (western Alps, Italy). *Eur J Miner* 1:89–104
- Pognante U, Kienast JR (1987) Blueschist and eclogite transformations in Fe-Ti gabbros: a case from the Western Alps Ophiolites. *J Petrol* 28:271–292
- Poli S, Schmidt MW (1997) The high-pressure stability of hydrous phases in orogenic belts: an experimental approach on eclogite forming processes. *Tectonophysics* 273:169–184
- Poli S, Schmidt MW (2002) Petrology of subducted slabs. *Annu Rev Earth Planet Sci* 30:207–235
- Pouchou JL, Pichoir F (1985) “PAP”  $\phi(\rho Z)$  procedure for improved quantitative microanalysis. In: Armstrong JT (ed) *Microbeam Analysis*. San Francisco Press, San Francisco, CA, pp 104–106
- Proyer A, Rolfo F, Zhu Y-F, Castelli D, Compagnoni R (2013) Ultrahigh-pressure metamorphism in the magnesite + aragonite stability field: evidence from two impure marbles from the Dabie-Sulu UHPM belt. *J Metamorph Geol* 31:35–48
- Reddy SM, Wheeler J, Cliff RA (1999) The geometry and timing of orogenic extension: an example from the Western Italian Alps. *J Metamorph Geol* 17:573–589
- Reddy SM, Wheeler J, Butler RWH, Cliff RA, Freeman S, Inger S, Pickles C, Kelley SP (2003) Kinematic reworking and exhumation within the convergent Alpine Orogen. *Tectonophysics* 365:77–102
- Reynard B, Ballèvre M (1988) Coexisting amphiboles in an eclogite from the Western Alps: new constraints on the miscibility gap between sodic and calcic amphiboles. *J Metamorph Geol* 6:333–350
- Saliot P (1973) Les principales zones de métamorphisme dans les Alpes françaises. Répartition et signification. *C R Acad Sci Paris* 276:3081–3084
- Sartori M (1987) Structure de la zone du Combin entre les Diablons et Zermatt (Valais). *Eclogae Geol Helv* 80:789–814
- Schmidt MW (1995) Lawsonite: upper pressure stability and formation of higher density hydrous phases. *Am Miner* 80:1286–1292
- Schmidt MW, Poli S (1994) The stability of lawsonite and zoisite at high pressure: experiments in CASH to 92 kbar and implications for the presence of hydrous phases in subducted lithosphere. *Earth Planet Sci Lett* 124:105–118
- Schmidt MW, Poli S (1998) Experimentally based water budgets for dehydrating slabs and consequences for arc magma generation. *Earth Planet Sci Lett* 163:361–379
- Schumacher JC, Brady JB, Cheney JT, Tonnsen RR (2008) Glaucophane-bearing marbles on Syros, Greece. *J Petrol* 49:1667–1686
- Schwartz S, Lardeaux JM, Tricart P (2000) La zone d’Acceglio (Alpes cottiennes): un nouvel exemple de croûte continentale écologitisée dans les Alpes occidentales. *C R Acad Sci* 330:859–866
- Seidel E (1977) Lawsonite-bearing metasediments in the phyllite-quartzite series of SW-Crete (Greece). *N Jb Miner Abh* 130:133–144
- Seaton NCA, Whitney DL, Teyssier C, Toraman E, Heizler MT (2009) Recrystallization of high-pressure marble (Sivrihisar, Turkey). *Tectonophysics* 479:241–253
- Shaw DM (1956) Geochemistry of pelitic rocks: Part III. Major elements and general geochemistry. *Geol Soc Am Bull* 67:919–934
- Snow E, Yund RA (1987) The effect of ductile deformation on the kinetics and mechanisms of the aragonite–calcite transformation. *J Metamorph Geol* 5:141–153
- Sotin C, Madon M (1988) Generalized nonlinear inversion of kinetics data: application to the calcite = aragonite transformation. *Phys Earth Planet Int* 52:159–171
- Sperlich R (1988) The transition from crossite to actinolite in metabasites of the Combin Unit in Vallée St. Barthelemy (Aosta, Italy). *Schweiz Miner Petrogr Mitt* 68:215–224
- Staudigel H (2014) Chemical fluxes from hydrothermal alteration of the oceanic crust. In: Rudnick RL (ed) *The Crust. Treatise on geochemistry*. Elsevier, Oxford, pp 583–606
- Tajčmanová L, Manzotti P, Alvaro M (2021) Under pressure: high-pressure metamorphism in the Alps. *Elements* 17:201–207
- Theye T, Seidel E (1993) Uplift-related retrogression history of aragonite marbles in western Crete (Greece). *Contrib Miner Petrol* 114:349–356
- Tinkham DK, Zuluaga CA, Stowell HH (2001) Metapelite phase equilibria modeling in MnNCKFMASH: the effect of variable  $Al_2O_3$  and  $Mg/(MgO+FeO)$  on mineral stability. *Geol Mater Res* 3:1–41
- Topuz G, Okay AI (2014) Prograde calcite to aragonite transformation in the Gümüşyeniköy micritic limestones (Tavşanlı, NW Turkey). *Int J Earth Sci* 103:2271–2272
- Topuz G, Okay AI, Altherr R, Meyer HP, Nasdala L (2006) Partial high-pressure aragonitization of micritic limestones in an accretionary complex, Tavşanlı zone, NW Turkey. *J Metamorph Geol* 24:603–613
- Tsujimori T, Ernst WG (2014) Lawsonite blueschist and lawsonite eclogites as proxies for palaeo-subduction zone processes: a review. *J Metamorph Geol* 32:437–454
- Ueno T (1999) REE-bearing sector-zoned lawsonite in the Sanbagawa pelitic schists of the eastern Kii Peninsula, central Japan. *Eur J Miner* 11:993–998
- Vance JA (1968) Metamorphic aragonite in the prehnite-pumpellyite facies, northwest Washington. *Am J Sci* 266:299–315
- Van der Molen I, van Roermund HLM (1986) The pressure path of solid inclusions in minerals: the retention of coesite inclusions during uplift. *Lithos* 19:317–324
- Vitale Brovarone A, Herwartz D (2013) Timing of HP metamorphism in the Schistes Lustrés of Alpine Corsica: new Lu-Hf garnet and lawsonite ages. *Lithos* 172–173:175–191
- Vitale Brovarone A, Beyssac O (2014) Lawsonite metasomatism: A new route for water to the deep Earth. *Earth Planet Sci Lett* 393:275–284
- Vitale Brovarone A, Alard O, Beyssac O, Martin L, Picatto M (2014a) Lawsonite metasomatism and trace element recycling in subduction zones. *J Metamorph Geol* 32:489–514
- Vitale Brovarone A, Picatto M, Beyssac O, Lagabrielle Y, Castelli D (2014b) The blueschist-eclogite transition in the Alpine chain: P-T paths and the role of slow-spreading extensional structures in the evolution of HP–LT mountain belts. *Tectonophysics* 615–616:96–121
- Vitale Brovarone A, Martinez I, Elmaleh A, Compagnoni R, Chaduteau C, Ferraris C, Esteve I (2017) Massive production of abiotic methane during subduction evidenced in metamorphosed ophicarbonates from the Italian Alps. *Nat Commun* 8:14134
- Vitale Brovarone A, Tumiami S, Piccoli F, Ague JJ, Connolly JA, Beyssac O (2020) Fluid-mediated selective dissolution of subducting carbonaceous material: implications for carbon recycling and fluid fluxes at forearc depths. *Chem Geol* 549:119682
- Wei CJ, Powell R (2004) Calculated phase relations in high-pressure metapelites in the system NCKFMASH ( $Na_2OK_2O-FeO-MgO-Al_2O_3-SiO_2-H_2O$ ). *J Petrol* 45:183–202
- White RW, Powell R, Holland TJB, Worley B (2000) The effect of  $TiO_2$  and  $Fe_2O_3$  on metapelitic assemblages at greenschist and amphibolite facies conditions: mineral equilibria calculations in the system

$K_2O$ – $FeO$ – $MgO$ – $Al_2O_3$ – $SiO_2$ – $H_2O$ – $TiO_2$ – $Fe_2O_3$ . *J Metamorph Geol* 18:497–511

White RW, Pomroy NE, Powell R (2005) An in-situ metatexite-diatexite transition in upper amphibolite facies rocks from Broken Hill, Australia. *J Metamorph Geol* 23:579–602

Whitney DL, Fornash KF, Kang P, Ghent ED, Martin L, Okay AI, Vitale Brovarone A (2020) Lawsonite composition and zoning as tracers of subduction processes: a global review. *Lithos* 370–371:105636

Zwart HJ (1962) On the deformation of polymetamorphic mineral associations and its application to the Bosost area (Central Pyrenees). *Geol Rund* 52:38–65

**Publisher's Note** Springer Nature remains neutral with regard to jurisdictional claims in published maps and institutional affiliations.